High-resolution impact assessment of climate change on building energy performance considering extreme weather events and microclimate –

Sustainable Cities and Society 78 (2022) 103634

Contents lists available at ScienceDirect

Sustainable Cities and Society

journal homepage: www.elsevier.com/locate/scs

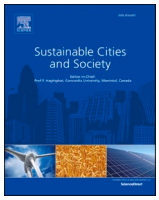

High-resolution impact assessment of climate change on building energy performance considering extreme weather events and microclimate – Investigating variations in indoor thermal comfort and degree-days

Mohammad Hosseini [a,b], Kavan Javanroodi [c,d], Vahid M. Nik [b,c,*]

[a] Department of Ocean Operations and Civil Engineering, Faculty of Engineering, NTNU Norwegian University of Science and Technology, Ålesund, Norway
[b] Division of Building Physics, Department of Building and Environmental Technology, Lund University, SE-22363 Lund, Sweden
[c] Division of Building Technology, Department of Architecture and Civil Engineering, Chalmers University of Technology, SE-41296 Gothenburg, Sweden
[d] Solar Energy and Building Physics Laboratory (LESO-PB), Ecole Polytechnique Fédérale de Lausanne (EPFL), CH-1015 Lausanne, Switzerland

ARTICLE INFO

Keywords:
Climate change adaptation
Extreme climate events
Urban microclimate
Urban heat island
Indoor thermal comfort
Building energy performance

ABSTRACT

Climate change and urbanization are two major challenges when planning for sustainable energy transition in cities. The common approach for energy demand estimation is using only typical meso-scale weather data in building energy models (BEMs), which underestimates the impacts of extreme climate and microclimate variations. To quantify the impacts of such underestimation on assessing the future energy performance of buildings, this study simulates a high spatiotemporal resolution BEM for two representative residential buildings located in a 600 × 600 m2 urban area in Southeast Sweden while accounting for both climate change and microclimate. Future climate data are synthesized using 13 future climate scenarios over 2010-2099, divided into three 30-year periods, and microclimate data are generated considering the urban morphology of the area. It is revealed that microclimate can cause 17% rise in cooling degree-day (CDD) and 7% reduction in heating degree-day (HDD) on average compared to mesoclimate. Considering typical weather conditions, CDD increases by 45% and HDD decreases by 8% from one 30-year period to another. Differences can become much larger during extreme weather conditions. For example, CDD can increase by 500% in an extreme warm July compared to a typical one. Results also indicate that annual cooling demand becomes four and five times bigger than 2010-2039 in 2040-2069 and 2070-2099, respectively. The daily peak cooling load can increase up to 25% in an extreme warm day when accounting for microclimate. In the absence of cooling systems during extreme warm days, the indoor temperature stays above 26°C continuously over a week and reaches above 29.2°C. Moreover, the annual overheating hours can increase up to 140% in the future. These all indicate that not accounting for influencing climate variations can result in maladaptation or insufficient adaptation of urban areas to climate change.

1. Introduction

Urban areas accommodate more than half of the world's population (Mihaela, 2014), expected to rise to more than two-thirds by 2050 (Sethi et al., 2021). They are also counted as the primary source of greenhouse gas emissions in different sectors (Revi et al., 2014), whereas more than 70% of the CO_2 emissions for energy use are emitted in urban areas (Seto et al., 2014). Numerous local and international policies have been conducted to control and reduce the environmental impacts of urbanization. The Sustainable Development Goal (SDG) 11 of the United Nations Agenda 2030 (sustainable cities and communities) has explicitly defined the reduction of environmental impacts (Target 11.6) and the resource efficiency and resilience of cities (Target 11.b) as indicators to reach the defined sustainable goals (UN, 2015). SDG 3 (good health and well-being) and SDG 7 (affordable and clean energy) are strongly connected to urban energy solutions and sustainable transition. Furthermore, it is vital to reduce anthropogenic climate changes to limit the global average temperature rise well below 2°C above the pre-industrial level (Nik et al., 2021). The Paris Agreement mandates countries to take action toward the climate goals (Rogelj et al., 2016), which is emphasized in SDG 13 (climate action).

A fundamental goal of urban energy solutions is to enhance human comfort, in which a considerable weight is on providing indoor thermal comfort. The effects of high-temperature periods, so-called heatwaves, have been experienced since the 2003 heatwave in western European

* Corresponding author:
E-mail addresses: mohammad.hosseini@ntnu.no (M. Hosseini), kavan.javanroodi@epfl.ch (K. Javanroodi), vahid.nik@byggtek.lth.se (V.M. Nik).

https://doi.org/10.1016/j.scs.2021.103634
Received 29 September 2021; Received in revised form 9 December 2021; Accepted 20 December 2021
Available online 23 December 2021

Nomenclature

ASHRAE	American Society of Heating, Refrigerating and Air-Conditioning Engineers
BEM	Building energy model
CDD	Cooling Degree-Day
CV(RMSE)	Coefficient of Variation of Root Mean Square Error
DHW	Domestic Hot Water
DOE	Department Of Energy
ECY	Extreme Cold Year
EPS	Energy Performance Simulation
EWY	Extreme Warm Year
FEMP	Federal Energy Management Program
$\widehat{g}(t)$	Kernel estimate for time t
GCM	Global climate model
GIS	Geographic Information System
h	The bandwidth of the kernel
HDD	Heating Degree-Day
HVAC	Heating, Ventilation, and Air Conditioning
i	Index of values in demand data time series
IPCC	Intergovernmental Panel on climate change
$K(u)$	Gaussian kernel function
LoD	Level of Detail
n	Length of the demand data time series
NMBE	Normalized Mean Bias Error
OSM	Open Street Map
Q_i	Measured demand at index i in time series
RCM	Regional Climate Model
RCP	Representative Concentration Pathway
RD	Relative Difference
SDG	Sustainable Development Goal
SH	Space Heating
SMY	Synthesized Meteorological Year
T_t	Temperature at time t *in an hourly scale*
TDY	Typical Downscaled Year
TMY	Typical Meteorological Year
UHI	Urban Heat Island
$\overline{y}$	Mean values of the measured data
$\widehat{y}_i$	Simulated hourly data at index i
y_i	Measured hourly data at index i
ΔT_d	Daily average temperature difference between meso- and microclimate conditions
ΔT_h	The temperature difference between meso- and microclimate conditions at the h^{th} hour of the day (0-23)

countries (with a high mortality rate) followed by several other extreme warm summers (Robine et al., 2008). Elderly people, patients suffering from cardiovascular disease, diabetes, and other chronic illnesses are at severe risk of extreme warm temperatures (Schwartz, 2005); where July 2021 has earned the unenviable distinction as the world's hottest month ever recorded, narrowly beat July 2016, 2019, and 2020 (NOAA, 2021). The fact that all these peaks have occurred recently, which can be considered to be in a statistical tie for Earth's hottest months (Masters, 2021), accentuates impacts of climate change. Furthermore, due to climate change, a higher number of extreme weather events are expected in the future (Chen et al., 2018), with higher frequencies and stronger magnitudes affecting both the energy demand and supply (Perera et al., 2020). Such extreme events and the consequent cascading failures can put unprecedented extra loads on energy systems, disrupt the proper functioning of buildings and energy systems and risk the thermal comfort and health of people. Unpredicted and unexpected climate shocks cause energy supply poverty in urban areas where households cannot supply their energy (Jessel et al., 2019; Thomson et al., 2019). Moreover, the economic effects of climate extremes are also significant at different scales, such as impairment of energy systems (Cronin et al., 2018), increased healthcare costs (Gasparrini et al., 2015; Jessel et al., 2019), power outages as well as disturbances in crucial modern days platforms (Campbell, 2013; Kenward & Raja, 2014).

Climate shocks influence the performance of urban energy systems on both the demand (Yang et al., 2021) and supply (Perera et al., 2020) sides. On the supply side, although moving towards higher integration of renewable energy sources contributes effectively to the urban area's sustainability, adapting to climate change is still essential since renewable energy production is highly influenced by climate variations (Nik, 2016; Perera et al., 2020). As a major part of the demand side and responsible for providing indoor thermal comfort, buildings play a significant role in reaching flexible and resilient urban energy solutions (Nik et al., 2021; Nik & Moazami, 2021). Therefore, having a reliable and accurate assessment of the energy performance of buildings is required to properly plan for climate change adaptation in urban areas (Nik & Moazami, 2021).

Multiple approaches have been developed and are adopted for energy performance estimation (Amasyali & El-Gohary, 2018; Wei et al., 2018; Zhao & Magoulès, 2012). Engineering methods, among all developed approaches, provide a comprehensive, detailed estimation through Energy Performance Simulation (EPS) (Sousa, 2012; Zhao & Magoulès, 2012). However, the building sector severely suffers from the shortage of high-resolution measured energy and indoor climate data as well as reliable predictions of future conditions, especially during extreme climate events. Significant uncertainties also exist for the current process (Walch et al., 2020; Nik & Sasic Kalagasidis, 2013). The more uncertain inputs are, the more unrealistic EPS results will be (Bhandari et al., 2012), which can cause discrepancies from 30% up to 100% from actual energy performance (Ioannou & Itard, 2015).

The accuracy of EPS relies upon several parameters/variables, especially those related to (1) outdoor weather (Erba et al., 2017), (2) building energy modeling (BEM) (Menberg et al., 2016), and (3) urban modeling (Javanroodi et al., 2018). The quality of weather data defines the accuracy of the outdoor condition as the primary boundary condition for the model; however, historical weather data are not available for every selected place and site around the globe. Typical Meteorological Year (TMY) weather data are commonly used for energy simulation, representing the most common monthly conditions among multiple years (usually 30 years)(Janjai & Deeyai, 2009). Accordingly, the TMY file differs from the actual measured data over a certain year (Tsoka et al., 2017). A drawback of using TMY data is that it fails to address the probable extreme weather conditions (Crawley, 1998). This becomes critical when the plan is increasing climate change adaptation in the future (Nik, 2016). Furthermore, it is crucial to consider extreme situations when considering climate resilience and system sizing (Nik et al., 2021). Hence, Synthesized Meteorological Year (SMY) (Cui et al., 2017) needs to be adopted to achieve higher accuracy and provide future weather data with extreme conditions based on various scenarios (Nik, 2016, 2017).

BEM can be divided into building geometry and building performance. The geometry accuracy depends on the precision of parameters to represent shapes and dimensions, glaze to wall ratio, effective surface area, and relative compactness (Bourisli et al., 2018; Y. Huang & Li, 2021). Building performance is intrinsically involved with uncertainties, including user behavior, occupancies, and envelope quality (Ding et al., 2015; Tian et al., 2018). These uncertainties cause deviations in EPS results, particularly influencing hourly profiles, where the hourly trend evaluates thermal comfort (Kallert et al., 2018; Kensby, 2015) and defines the peak power. Nevertheless, EPS hourly results can be calibrated with the hourly measurements to eliminate the effects of uncertainties,

minimize discrepancies from measured profiles, and have a realistic assessment of indoor conditions.

Developing the urban morphology model, including surrounding buildings, trees, and vegetation, has considerable effects on the accuracy of EPS models (Javanroodi, 2018; Perera et al., 2021a). Anthropogenic heat emissions from human activities also affect the local weather conditions, and consequently, the EPS models (Lee et al., 2020). Thus, a wide range of uncertainties would emerge due to a large number of influencing parameters as well as the complexity of local climate measurements. It is crucial to model significant urban elements for EPS. However, the accuracy of the urban modeling would be satisfied with the level of detail (LoD) of 1 or 2 (Goy et al., 2020), where buildings are modeled as simple extruded blocks with flat roofs or simple-inclined roofs (Biljecki, 2017; Biljecki et al., 2016).

The aggravated impacts of climate change and urban morphology on building energy performance has been assessed by Berardi and Jafarpour (2020) using two dynamically downscaled global climate models (GCM) for typical weather conditions and performing EPS on 16 reference building models developed by the United States Department of Energy (DOE). Li et al. (2021) and Gao et al. (2022) have calculated the effects of the urban heat island (UHI) as a function of urban morphology, using a geographically weighted regression model. Khoshnoodmotlagh et al. (2021) has evaluated the UHI effects on the accuracy of satellite imagery. Wang & Shu (2021) have assessed future climate and UHIs on building energy performance using monitored data, on-site surveying, and EPS with calibrated models. Berardi and Jafarpour (2020), Mourshed (2011), and Taha (1997) have used the concept of heating degree-day (HDD) and cooling degree-day (CDD) as a metric to quantify the impacts of UHI. The applicability of using opensource geographical information system (GIS) data for urban energy modeling is assessed by Wang et al. (2021), where buildings' footprints are captured from OpenStreetMap (OSM), and building height for residential buildings are defined based on the story number. Schiefelbein et al. (2019) show the credibility of urban and building energy modeling using geometry from OSM, enriched by building stock statistics as the building performance. Zhou et al. (2021) has performed an impact assessment of UHI and future climate on health risks using urban morphology parameters, including sky view factors, permeable surface fraction, building surface fraction, and building height.

More than the aforementioned studies, several other studies have been conducted to forecast the energy demand and thermal comfort of buildings and prepare buildings' owners and district energy providers with reliable predictions (Biswas et al., 2016; Deb et al., 2017; Massana et al., 2015; Zhao & Magoulès, 2012). However, there is a gap in performing hourly assessments, considering extreme climate events based on the high-resolution temporal and spatial measured data in both building and urban scale. There is no high-resolution assessment of the impacts of climate extremes on the energy performance of buildings and their indoor comfort, considering both the temporal and spatial resolutions at the urban and building scales (i.e. considering microclimate conditions around buildings and multiple climate zones inside buildings). This work contributes to the field by conducting a high spatio-temporal resolution impact assessment of climate change on the energy performance of buildings and their indoor comfort, considering a comprehensive set of hourly future weather data and simulating a detailed BEM. The impacts of climate change on microclimate, with specific focus on extreme conditions are evaluated, comparing outdoor temperature and degree-days when using only mesoclimate and when simulating microclimate for the considered urban area based on the same mesoclimate data. Such a detailed impact assessment is performed for two residential buildings in Karlshamn, Sweden. In this regard, a set of hourly scale synthesized future weather data, generated by downscaling 13 GCMs, is used in addition to representative weather data sets for typical and extreme conditions (generated based on the developed method by Nik (2016)), all for three 30-year periods over 2010-2099. A BEM is developed and verified against high-resolution measured energy use and temperature for the indoor and outdoor spaces of the considered buildings. The BEM considers the urban morphology through importing urban elements and landscape from GIS to the BEM, accounting for microclimate effects. Aggravated impacts of climate change and urban morphology, particularly in extreme weather conditions, on building energy performance and indoor thermal comfort are quantified in a high-resolution time scale.

This study is organized as follows. In Section 2, the methodology of developing BEM and performing EPS using future weather data are discussed. Section 3 thoroughly assesses the results, followed by conclusions of the research in Section 4.

2. Methodology

The research work is based on the energy modeling of two residential buildings, using detailed geometry and measured data for heating demand, indoor- and outdoor temperature over a year. The workflow is divided into two time periods of past and future, as depicted in Fig. 1. The past conditions were used as the reference for calibration of the BEM to acquire a realistic model. Then, based on the verified model, future conditions were estimated using EPS and applying a broad spectrum of future weather scenarios to assess long and short-term impacts of climate change, including typical and extreme conditions.

This section will explain the (1) selected case study, including buildings and their specifications, (2) adopted approach to account for demand separation, (3) past and future weather data sets, including typical and extreme years used in energy simulations, (4) analysis of microclimate conditions in the considered area, (5) developed building energy models, (6) applied techniques for modeling calibration and verification, and (7) simulation progress and general workflow.

2.1. Case study

A neighborhood including two multi-family residential buildings in Karlshamn is selected as the case study, located in the middle of Sweden's Southeast coast, defined as warm temperate climate and fully humid with cool summer, according to Köppen and Geiger climate classification (Kottek et al., 2006). According to the Official Statistics of Sweden, more than 50% of the entire population lives within 10 km and 14% within 1 km of coastline (SCB, 2019). Buildings were constructed before the 1930s and have been renovated partially during different periods. According to the Swedish Statistic Organization, more than 12% of the current buildings are built before the 1930s (SCB, 2017). The neighborhood is located in a low-density urban area where the surrounding buildings are mostly three-story residential buildings with a basement and attic. The 600 $\times$ 600 m^2 surrounding urban area is modelled to account for microclimate conditions, which is explained in 2.4. Buildings are connected to the district heating system through one shared node for heating purposes and have no cooling system installed. Table 1 presents some of the physical specifications of buildings, and Fig. 2 illustrates 3D models of the buildings and surrounding urban elements and landscape.

A high-resolution set of measured data is provided for the buildings consisting of (1) supplied heat from the district heating system to cover the space heating (SH) and domestic hot water (DHW) demands, (2) outdoor temperature, and (3) indoor temperature per room. Data is recorded every 15 minutes (4 records per hour) over one year starting from 01-01-2016. The total recorded heating demand for both buildings equals 151,200 kWh, equivalent to ~170kWh/m^2 for conditioned areas.

2.2. Demand separation

Heating demand is measured via one meter on the total supplied heat from district heating and includes SH and DHW. Since this research is focused on SH demand, a non-parametric method is applied to exclude the DHW from the total hourly demand. This method exploits a statis-

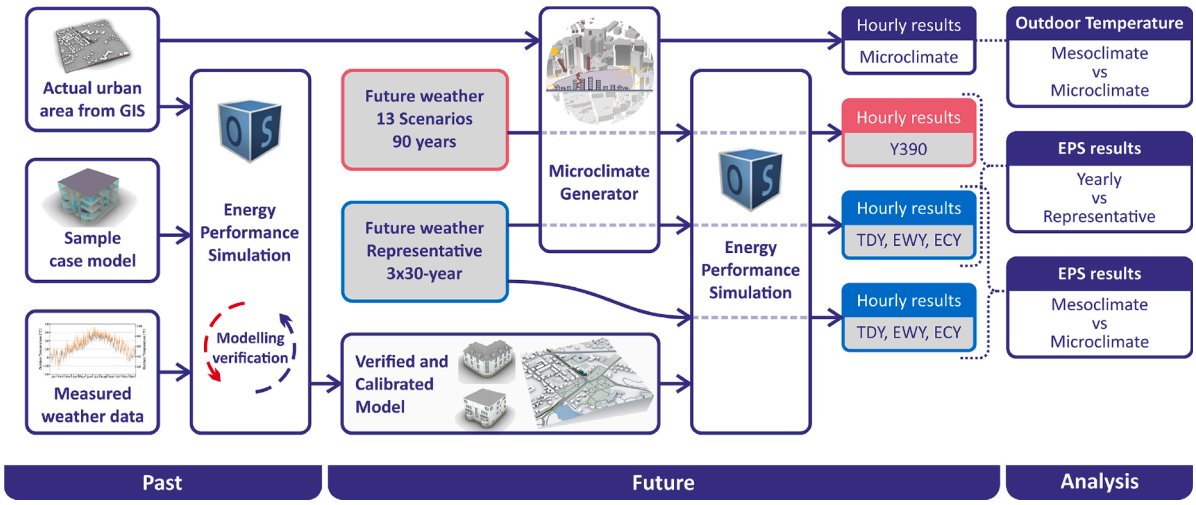

Fig. 1. The workflow for the proposed method; divided into Past and Future, which Past is based on high resolution measured energy and climate data, and Future is for estimating the energy performance of buildings for the future climate (more details about future weather data are available in Fig. 3 and Fig. 4).

Table 1
Buildings physical specifications.

	Building A	Building B
Total floor area [m^2]	670	655
Conditioned area [m^2]	455	442
Number of floors	3	3
Number of apartments	6	3
Number of rooms	26	18
Windows area [m^2]	69	58
Glazing area	44	41
Envelope / Total floor area	1.37	1.16
Windows to wall ratio	17%	15%
Glazing to wall ratio	11%	11%

tical time series approach based on a kernel smoothing technique (Bacher et al., 2016) to determine the fundamental data in a noisy data set. DHW load appears as spikes due to the intensive high demand of DHW in a short period, while SH has slow changes and a smooth pattern (Pezzutto et al., 2019). In Eq. (1), $\widehat{g}(t)$ is the kernel estimate for time t, n is the length of time series which is iterated by i, Q_i is the measured demand in the i^{th} index of the time series, k is a Gaussian kernel function defined as $k(u) = (2\pi)^{-1} \bullet \exp\{-0.5 \bullet u^2\}$. Moreover, h is the bandwidth of the kernel, while in the developed method by Bacher et al. (2016), h is not defined since the bandwidth can be adjusted based on the different kinds of datasets as well as desired accuracy and speed of the calculation. In this study, h equals to 4 in the hourly time step.

$$\widehat{g}(t) = \sum_{i=1}^{n} \frac{Q_i \cdot k\left(\frac{t-i}{h}\right)}{\sum_{i=1}^{n} k\left(\frac{t-i}{h}\right)} \tag{1}$$

2.3. Weather data

Two groups of weather data are used in this work representing past and future climate. The past climate data contains historical data and in-situ measurements. The future climate data is synthesized data from multiple future climate scenarios, which are explained further.

The past climate is used in EPS for the existing condition by exploiting a standard EPW file. The weather data file is TMY type for a

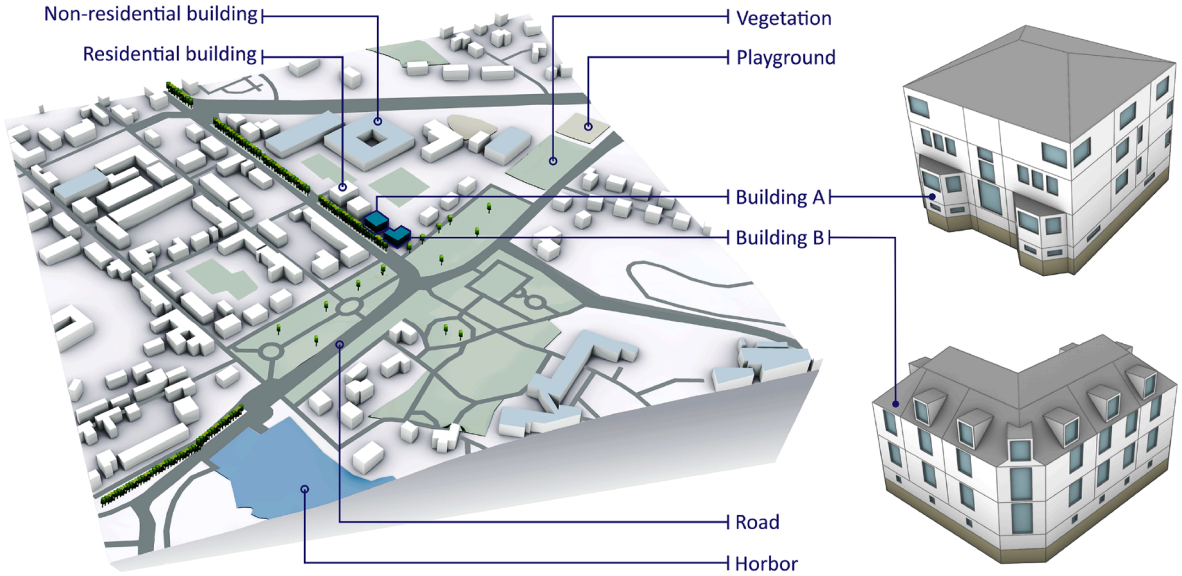

Fig. 2. The 3D model of the urban area that considered as urban morphology to generate microclimate data (left) and the sample buildings selected for high resolution energy performance assessment (right).

meteorological station within an appropriate distance (Crawley, 1998; EnergyPlus, 2021) (below 30km) with an annual average of the dry-bulb temperature of 7.9°C. However, in the measurement period, the annual average is recorded as 9.9°C. Thus, the EPW file is modified using the measured outdoor dry-bulb temperature to better represent the actual weather conditions. Using the measured temperature also helps to better account for the impacts of the urban morphology on climate conditions as microclimate.

Future climate in this study is generated using climate data from the RCA4 regional climate model (RCM), dynamically downscaling five GCMs forced by three representative concentration pathways (RCPs). GCMs may simulate different responses to the same forcing (Nik, 2016); hence, utilizing a number of them could a more reasonable distribution for future weather projections. In this study, five GCMs are applied, namely, CNRM-CM5, ICHEC-EC-EARTH, IPSL-CM5A-MR, MOHC-HadGEM2-ES, and MPI-ESM-LR. RCP includes time series of emissions and concentration of GHG, chemically active gases, and aerosols. Among many different pathways, Intergovernmental Panel on climate change (IPCC) used RCP 2.6 (stringent mitigation scenario), RCP 4.5 and 6.5 (intermediate stabilization pathways), and RCP 8.5 (high pathway) for its reports assessments (Good et al., 2012). In this research, CNRM-CM5 and IPSL-CM5A-MR are forced with RCP 4.5 and 8.5, and the rest are also forced with RCP 2.6 in addition to RCP 4.5 and 8.5. In total, 13 climate scenarios are used in this research from 2010 to 2099. The 90-year period is divided into three 30-year periods, representing climate conditions at the beginning, middle, and end of the century. Therefore, each time stage is represented by 30 years of data for 13 climate scenarios, resulting in 390 years of data, also mentioned as Y390 in this research (check (Nik, 2016) for details). The graphical structure of the synthesized future weather is illustrated in Fig. 3.

In addition to the RCM data sets, representative weather data sets are synthesized for the purpose of this work based on the method developed by Nik (2016). The representative weather data contained three one-year climate data sets for each 30-year period, including typical downscaled year (TDY), extreme warm year (EWY), and extreme cold year (ECY), as schematically presented in Fig. 4. These data sets are synthesized considering all the 13 future climate scenarios. Consequently, a wide range of climate variations and uncertainties (at the hourly temporal resolution) have been considered.

Applying the representative weather datasets enables us to decrease the number of simulations considerably (i.e. running three sets of one-year simulations instead of 390 years) without neglecting the impacts of climate uncertainties and extreme conditions. The application and accuracy of the representative weather data sets have been tested and verified for different types of simulations, including building energy performance (Moazami et al., 2019), hygrothermal performances of building components (Nik, 2017), and urban energy systems (Perera et al., 2020). The annual analyses based on extreme weather data sets represent pessimistic scenarios which are unlikely to happen since ECY and EWY respectively accumulate the extreme cold and warm months over a year. However, they provide a scientifically valid picture about probable future conditions on the monthly scale and finer. Therefore, for

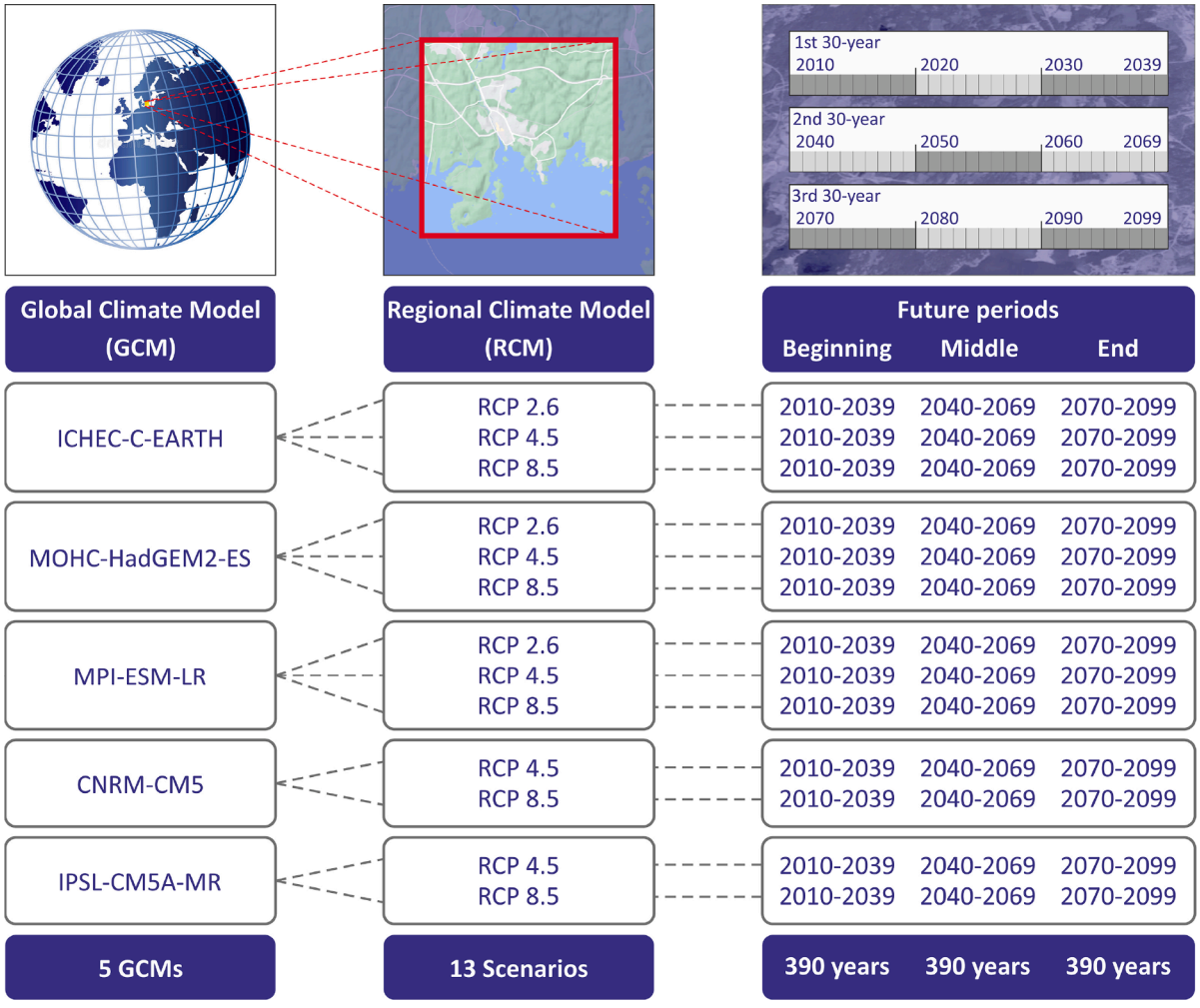

Fig. 3. For future climate conditions, climate big data sets with the hourly temporal resolution were synthesized for three 30-year periods using the RCA4 regional climate model and downscaling five global climate models forced by three different representative concentration pathways (check (Nik, 2016) for details).

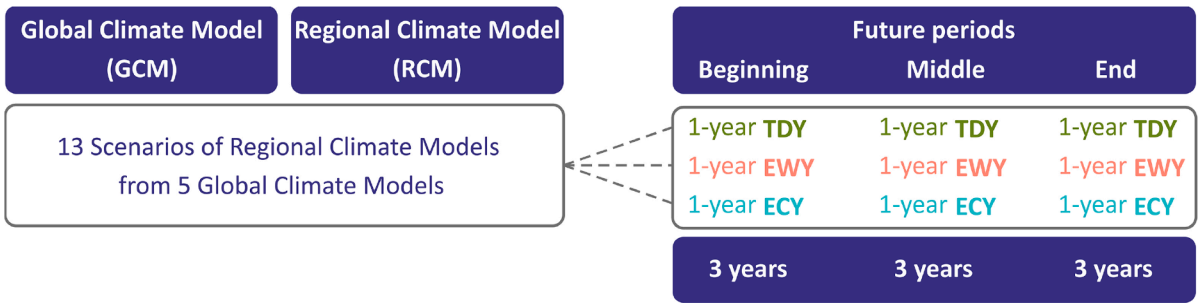

Fig. 4. Structure of the synthesized representative future weather data (check (Nik, 2016) for details).

extreme conditions results are discussed over shorter periods while the annual analyses are mainly made using TDY weather data. Some statistics about the representative weather data sets for the three 30-year periods are presented in Table 2. The readers are referred to (Nik, 2016) for more details about synthesizing representative weather data sets for future climate.

2.4. Microclimate modelling

The energy performance of buildings and bioclimatic metrics are influenced significantly by microclimate conditions (Javanroodi & Nik, 2019). Several morphological characteristics such as urban form, albedo, and vegetation density modify sky view factor (Taha, 1997), solar gain (Ma et al., 2020), solar reflectivity (Zoras et al., 2017), air temperature (Javanroodi & Nik, 2020), and wind speed (Javanroodi et al., 2021) within an urban area. In particular, for an urban area, lower average wind speed and higher average air temperature are expected compared to rural areas (Battista et al., 2021). The higher effective thermal inertia in the city, arising from larger surface areas with more heat capacities, causes a reduction in the diurnal cycle of air temperature (Ryu & Baik, 2012).

A high-resolution urban model is crucial in this research to account for the interactions between urban morphology and climate variables. In this regard, a detailed urban model is generated based on the OSM database. OSM database for selected case study provides building footprints, terrain, vegetation, building types, roads, and trees. In addition to the residential buildings, commercial buildings, offices, stadiums, and theatres are the main building types, combined as non-residential buildings in Fig. 2 for the sake of simplicity. However, buildings' heights and altitudes are not available for the target coordination. Thus, building footprints are projected to the terrain's mesh to locate them in the actual altitudes. Then, buildings' heights are defined from Google Street View based on the number of floors. Then, a 600 × 600 m^2 area around the target buildings is modeled, including 192 blocks (nearly 90% residential and 10% non-residential). Finally, parks, playgrounds, green areas, and roads are modeled in the considered area. The urban model has not considered dynamic changes in plants and trees as well as the real surface of the roads.

The applied energy simulation engine, EnergyPlus, does not calculate the local wind speed and air temperature under the effects of the urban morphology and uses the meteorological data from the EPW file (Ellis & Torcellini, 2005). DragonFly plugin for Grasshopper is adopted to generate the microclimate weather data, using the Urban Weather Generator (UWG) method. UWG estimates the effects of UHI by using the energy conservation principles to account for the effects of the urban canopy and boundary layers on microclimate conditions (Bueno et al., 2014). UWG solves the effects of surface roughness on flow by using the vertical air temperature profile calculated by the vertical diffusion sub model and a logarithmic profile for the wind speed (Bueno et al., 2012). The anthropogenic heat gains are considered by energy performance estimation of buildings using their type and area. The lower evaporation because of the reduction in vegetation area is also applied by the vegetation surface coverage ratio (Bueno et al., 2013). UWG divides the entire urban model into different modules to consider the interaction between neighborhoods, so-called urban mapping. The urban mapping method defines each module as upwind and downwind for the adjacent modules based on the wind direction (considered in four quadrants). Thereafter, the average boundary layer air temperature is calculated for each time step (of the observed meteorological data) and assigned to the next neighborhood as the reference temperature (Bueno et al., 2014).

Additionally, the shading effects and reflectance of buildings are considered using True View Factor in EnergyPlus. Shading objects can also cast shadows on the ground, reducing the ground-reflected radiation (Perera et al., 2021a). Detailed surface geometry with the assigned material and reflectance is used to calculate the magnitudes and directions of shadings and reflectance by exploiting direct solar radiation and diffuse sky radiation from the modified weather file (Naboni et al., 2019).

Previous studies show various effects of UHI for the daytime and nighttime as well as different seasons (Rizwan et al., 2008; Taha, 1997); thus, UHI's impacts are studied seasonally in addition to daytime and nighttime. The difference between mesoclimate and microclimate conditions is defined in this research as $\Delta T_t = T_{tmicro} - T_{tmeso}$, where T_t is the temperature at time t in an hourly timestep. The average temperature difference for a day was also defined as ΔT_d to quantify the more extended span changes to eliminate the effects of single index peaks. Meaning that changes in one day would be considered. Therefore, ΔT_d is defined according to Eq. (2) where ΔT_h is ΔT at h^{th} hour of the day.

Table 2
Dry-bulb temperature distribution for the representative weather files.

	2010-2039			2040-2069			2070-2099		
	TDY	EWY	ECY	TDY	EWY	ECY	TDY	EWY	ECY
mean	7.9	12.1	1.8	8.6	13.3	2.8	9.4	14.5	3.6
SD	6.8	6.4	9.2	6.7	6.5	9.0	6.6	6.4	8.2
5%	-2.6	2.9	-14.5	-1.6	3.9	-13.1	-0.9	5.7	-10.2
25%	2.6	7.2	-4.4	3.5	8.0	-3.2	4.4	9.4	-2.1
50%	7.8	11.3	1.3	8.4	12.7	3.1	9.1	13.5	3.0
75%	13.3	16.5	10.1	13.9	17.8	10.5	14.6	19.2	10.8
95%	18.5	23.9	15.1	19.3	24.5	15.4	20.0	25.7	15.8

$$\Delta T_d = \frac{1}{24}\sum_{h=0}^{23}\Delta T_h \quad (2)$$

In this research, all future conditions EPSs are performed using microclimate weather data. In addition, the representative weather datasets for the mesoclimate and microclimate scale are utilized in EPS to assess the impacts of urban morphology on the indoor temperature and building energy performance in the future (see Fig. 6).

2.5. Building energy modeling

The building energy model is developed in Rhinoceros/Grasshopper via Ladybug and Honeybee plugins. A total number of 44 zones are created based on the buildings' blueprints and measurement datasheets to enable a detailed comparison. The urban model with the actual heights and altitudes is imported to the EPS through the EP_context component of Honeybee. The initial simulations are performed using past weather data and measured outdoor temperatures. The heating setpoints are imported as a list of hourly temperatures acquired from the median hourly temperature of each building. The indoor measured temperatures per room show high fluctuations because of user activities such as opening windows, altering local setpoints, sleeping, gathering, and/or changes in internal loads from lighting and equipment (Ueno & Meier, 2020).

The thermal transmittance coefficient (U-Value) is one of the most crucial parameters in EPS. It becomes even more critical for the traditional constructions where the U-value is higher than newly-built buildings. Energy simulation engines usually do not include traditional construction and material for U-value calculations, and in-situ measurement will be required instead (Baker, 2011). However, accurate measurement for existing building components is not straightforward because of the lack of information on actual constructions (Hulme & Doran, 2014). Moreover, similar constructions will have different performances after a long period of exposure to climate. Also, measurements are pretty sensitive to weather conditions and seasonal variations (Sørensen, 2013). Hence, a range of reasonable U-values is defined for exterior walls, roof, slab on the ground, basement walls, and windows based on similar cases (Baker, 2011; Hulme & Doran, 2014)]. Additionally, the infiltration rate through the envelope, which is hard to measure (P. Huang et al., 2015), is also considered as a range to calibrate the model due to its uncertain values (the calibration process is explained in 2.6). Infiltration is imported into the model based on the climate exposed surface area of the zone rather than air change per hour. Therefore, the number of exterior surfaces of each zone is considered in the simulation. Table 3 presents the U-value and infiltration rate of the buildings with the considered intervals.

To have a better representation of real conditions and user behavior, the operable windows were assumed to be opened when indoor temperature goes above 24°C, providing natural cooling during the warm hours where the cooling system is not installed (i.e. the only case with an installed cooling system is Building A for future climate). Moreover, the HVAC system does not work during the warm season (June 21st – September 21st). The number of occupants per floor area is calculated for each apartment based on the on-site surveying of the number of people, and the average is calculated for each building. Table 4 provides a brief overview of the main EPS parameters.

When running the energy simulations for future climate, the heating setpoint schedule was changed to the constant value of 21°C to eliminate the impacts of setpoint fluctuations when assessing results for future climate. For Building A (with a cooling system for future climate), the cooling setpoint was set to 26°C when running simulations for future climate. The setpoint is chosen according to FEBY (2019) which defines the overheating temperature above 26°C; therefore, the cooling setpoint is adjusted on this threshold to have a conservative energy efficiency attitude and do not overestimate the cooling demand in the future conditions. In contrast, no cooling system was assigned to Building B to evaluate the effectiveness of natural cooling in providing thermal comfort for future climate. The rest of the settings for the future conditions EPS were kept unchanged.

2.6. Model calibration and verification

The quality of a data-generative study relies upon accurate and unbiased energy models (Fan et al., 2021; FEMP, 2015), which is crucial for achieving reliable results (Burman & Mumovic, 2017). Well-recognized statistical methods in this order, which are also accepted by ASHRAE (ASHRAE Guideline 14, 2014) and FEMP, are the Coefficient of Variation of Root Mean Square Error (CV(RMSE)) and Normalized Mean Bias Error (NMBE), which were calculated based on the Eq. (3) (Fan et al., 2021) and Eq. (4) (Ruiz & Bandera, 2017), respectively. The accepted range of mentioned metrics is presented in Table 5. NMBE tends to eliminate errors (Burman & Mumovic, 2017; Ruiz & Bandera, 2017) since it takes the effect of negative and positive values into account, contrary to CV(RMSE), which does not cancel out errors. Hence, to avoid misleading implications, these two metrics should be used together, and both of them need to meet the criteria. In these equations $\hat{y}_i$ stands for the simulated hourly data at index i, y_i stands for the measured hourly data at index i, and $\bar{y}$ represents mean of the measured values. The calibration approach is to minimize the value of CV(RMSE) and NMBE by adjusting the results through alteration in U-value and infiltration rate mentioned in Table 4.

$$CV(RMSE) = 100 \times \frac{1}{\bar{y}} \cdot \sqrt{\left[\sum_{i=1}^{n} \frac{(y_i - \hat{y}_i)^2}{n}\right]} \quad (3)$$

$$NMBE = 100 \times \frac{\sum_{i=1}^{n}(y_i - \hat{y}_i)}{n \cdot \bar{y}} \quad (4)$$

2.7. Simulation procedure

EPS was performed separately for each building in Grasshopper with

Table 3
Calibration parameters interval and the adjusted values.

Parameter	Interval	Steps	Building A	Building B
Exterior walls U-value [W/m²•K]	0.8 – 1.6	0.1	1.3	1.1
Roof U-value [W/m²•K]	2.0 – 3.0	0.1	2.3	2.1
Slab on the ground U-value [W/m²•K]	0.8 – 1.6	0.1	1	0.8
Basement walls U-value [W/m²•K]	0.8 – 1.6	0.1	1.3	0.8
Windows U-value [W/m²•K]	1.0 – 3.0	0.1	1.3	1.2
Infiltration rate [l/m²•s]	0.8 – 2.0	0.1	1.2	1.2

Table 4
The main characteristics of the energy model.

Parameter	Building A	Building B
Conditioned zone [number]	26	18
VentilationPerPerson [l/s]	7	7
VentilationPerArea [l/s]	3	3
PeoplePerArea [people/m²]	0.019	0.012
Infiltration rate [l/m²•s]	1.2	1.2
Windows opening setpoint [°C]	24	24
mean U-Value [W/m²•K]	1.32	1.08
Heating setpoint [°C]	Varied (past climate) 21 (future climate)	Varied (past climate) 21 (future climate)
Cooling setpoint [°C]	Not assigned (past climate) 26 (future climate)	Not assigned (past climate) Not assigned (future climate)

Table 5
Model calibration and verification criteria.

Timestep	CV(RMSE)	NMBE
Hourly	<30%	<|±10%|

the OpenStudio simulation engine, exploiting EnergyPlus. Openstudio adds HVAC features to the EnergyPlus energy simulation engine (Crawley et al., 2008). A loop of EPS was employed to run a series of simulations based on the defined ranges of U-value and infiltration rate to reach the minimum calibration parameters (i.e. CV(RMSE) and |NMBE|). The loop iterated the list of U-value and infiltration. EPS hourly results were stored as CSV files, consisting of heating demand and zones temperatures. The calibration parameters were calculated based on the stored time-series in CSV files, as presented in Fig. 5. These simulations utilized measured weather data.

Future condition simulations used the calibrated model with future weather data, iterating the weather files by a loop of EPS as illustrated in Fig. 6. The results of simulations, including heating load, cooling load, and zones temperatures, were stored in a CSV file for every weather file. For each building, 1170 simulations were run with synthesized annual future weather data, in addition to nine simulations using the meso-climate representative weather data (ECY, TDY, and EWY) and nine simulations using microclimate representative weather data. Thus, in total, 1,188 years simulations were run, and the hourly results were stored. On average, each year EPS took five minutes on a PC with an Intel (TM) i7-4790K 4.00GHz CPU with 16.0 GB of RAM.

The 95th percentile of heating and cooling powers are considered the peak load and extreme conditions for energy demand. Hence, to investigate the hourly results for the extreme conditions, one week in summer and one week in winter are chosen, including the peak power. Having such criteria, the extreme warm summer week starts from July 10, and the extreme cold winter week starts from February 14.

3. Results and Discussion

3.1. Model verification and validation

Parameters of verification and validation of the EPS model based on the zones' temperatures are presented in Table 6 and Fig. 7, annually and seasonally. The required values for CV(RMSE) and NMBE (Presented in Table 3) are shown by the red lines on the box plots, which show that all zones are in the required range.

The similar range of the seasonal values of CV(RMSE) means that the model is well-calibrated in different seasons, and it can represent various conditions, for example, different temperatures or HVAC settings. Moreover, the symmetrical NMBE values to zero show that different zones have different degrees of under- and overestimation of the actual condition; therefore, the positive and negative deviations eliminate each other to some extent. Hence, the total simulated heating demand is close to measured values, whereas the annual hourly profile for the measured and simulated heating demand gives a CV(RMSE) of 23% and an NMBE of 4%. As a result, BEM is also calibrated and verified based on the hourly heating demand (see Fig. 17).

Two indoor dry-bulb temperature samples from each building are illustrated in Fig. 8 to show the measured values (blue line) against the simulated hourly profile (orange line). The graph shows a higher temperature in simulated values in May and June due to two phenomena. First, direct solar radiation into the rooms in EPS (southern windows), while it can be blocked by a curtain or other obstacle in actual condition. Second, it can result from underestimating the effects of natural ventilation in EPS compared to the actual condition since the rooms are toward the large open area in the south, and recorded wind data would not cover it precisely. Note that the constant temperature in October and party in June comes from the failure of the thermometer.

The applied separation method on the total hourly heating demand showed a value of nearly 9,000 kWh per year (530 kWh/year per person) for DHW, nearly 6% of the total heating demand. Fig. 9 shows the hourly measured heating demand (black line) and the separated spikes (blue line) as DHW for the summer- and winter week. The SH demand (red line) is the subtraction of the total demand (black line) from separated DHW (blue line). The summer week (left graph) shows the pattern of DHW demand while no SH is in progress to compare the output of the applied function for DHW demand separation, which presents a fairly similar pattern and intensity.

3.2. Microclimate weather data

The introduced future weather data in the previous chapter are compared with their corresponding microclimate data in Fig. 10 for three 30-year periods. Comparing the boxes for Y390 and Triple (which contains TDY, EWY, and ECY) shows that Triple can represent all 390 years of weather data with very high accuracy, very similar to the case of considering all 390 years without neglecting extreme events. TDY also represents the typical conditions very similar to Y390. The median line for Triple (long green line) is passed just above the median line for Y390 and TDY, and the same is also applied for 25th and 75th percentiles. Accordingly, their contents have a pretty similar distribution, so TDY can be used in EPS instead to reduce the number of simulations enormously (1 year instead of 390 years). Moreover, a comparison of the high and low boundaries shows that EWY and ECY cover the highest and lowest temperature range in Y390, which can help evaluate the extreme conditions without running a large number of simulations.

The distribution and differences (Diff.) of the meso- and microclimate conditions for the representative future weather data are presented in Table 7. EWY shows the most significant differences between meso- and microclimate with the increase of 0.6, 0.6, and 0.5 degrees Celsius of the average values in three periods, occurring due to the cumulative effects of the warm climate and the UHI effects.

The alterations in the outdoor air temperatures are not distributed equally either all around the year or over a day. Hence, a detailed analysis on a daily scale is required. Fig. 11 shows the seasonal outdoor

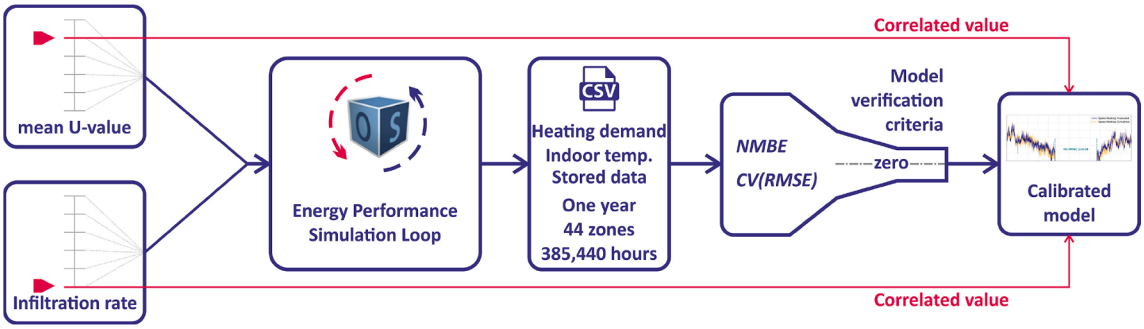

Fig. 5. Model calibration workflow including EPS loop and data storage.

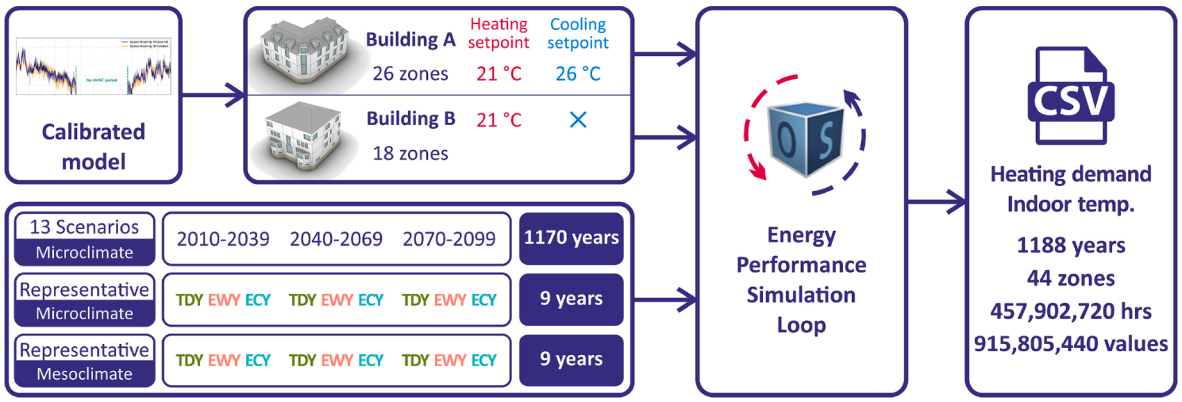

Fig. 6. Future conditions EPS and data storage workflow.

Table 6
Verification of the model with CV(RMSE) and NMBE for all zones' temperatures.

	Annual	spring	summer	autumn	winter	Annual	spring	summer	autumn	winter
mean	**4.66**	5.02	4.02	3.95	4.80	**0.23**	1.36	-0.48	0.00	0.14
STD	**1.45**	1.45	1.11	1.85	2.35	**2.71**	2.79	2.54	3.45	3.94
min	**3**	3	2	2	2	**-6**	-6	-6	-6	-10
max	**9**	9	7	9	11	**7**	7	4	9	10

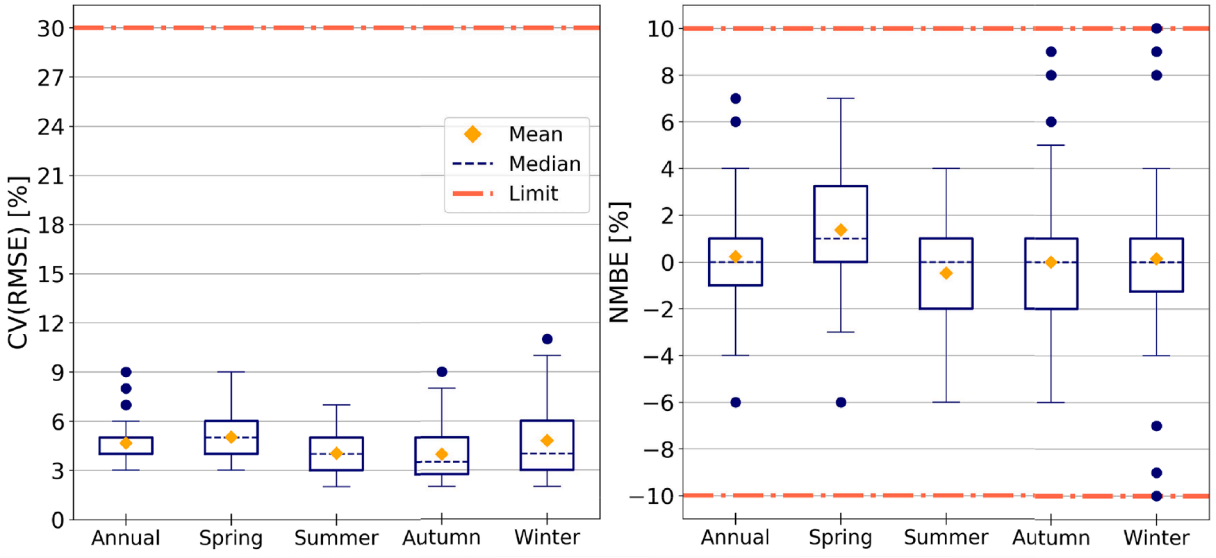

Fig. 7. Box plots for annual and seasonal CV(RMSE) and NMBE for all zones. Redlines indicate the requirements for each parameter.

temperature changes (ΔT) for TDY, EWY, and ECY over three future periods. The area of the bulbs represents the total ΔT (°C) for the season, while the white part in the middle shows the changes in the daytime (6:00 to 18:00); thus, the rest are related to nighttime (18:00 to 6:00). This chart shows firstly, dramatically higher ΔT for warm seasons, which is addressed in several previous studies (Rizwan et al., 2008), showing the larger effects of solar gain and albedo than anthropogenic heat gains in this specific urban morphology (Taha, 1997). Secondly, the impacts of UHI appeared fairly different from day to night. As illustrated in Fig. 11 (white area on each bulb), a small portion of ΔT happens between 06:00 and 18:00 (daytime), while the major part happens at nocturnal hours. In this case, above 95% of ΔT occurs at nighttime.

In Fig. 12 and Fig. 13, the hourly profiles of outdoor temperatures for microclimate (solid lines) and mesoclimate (dashed lines) in winter and summer weeks are presented. As expected, the differences between microclimate and mesoclimate are higher in spring and summer with an average of 0.7°C against 0.3°C in autumn and winter over 90 years for TDY. Moreover, the impacts of UHI emerge significantly at nighttime (grey zones), which has been reported by other studies, as well (Rizwan et al., 2008). The maximum outdoor temperature growth during daytime is 5.9°C, while it grows by a peak of 10.6°C during nighttime.

In the summer week (Fig. 13), the average ΔT (hourly difference between mesoclimate (solid line) and microclimate (dashed line) outdoor temperature) is 0.4°C and 0.9°C for TDY and 1.3°C and 1.7°C in EWY over 2040-2069 and 2070-2099, respectively.

Daily average temperature differences (ΔT_d) over three future periods are illustrated in Fig. 14 as duration diagrams, sorted by the values (not the time). The boxplots on the right show the distribution for all data from TDY, EWY, and ECY together, showing the possible bounds for daily temperature changes in typical and extreme conditions. Daily average temperature helps to assess the impacts of temperature change in a longer period (24 hours) instead of one single hour; therefore,

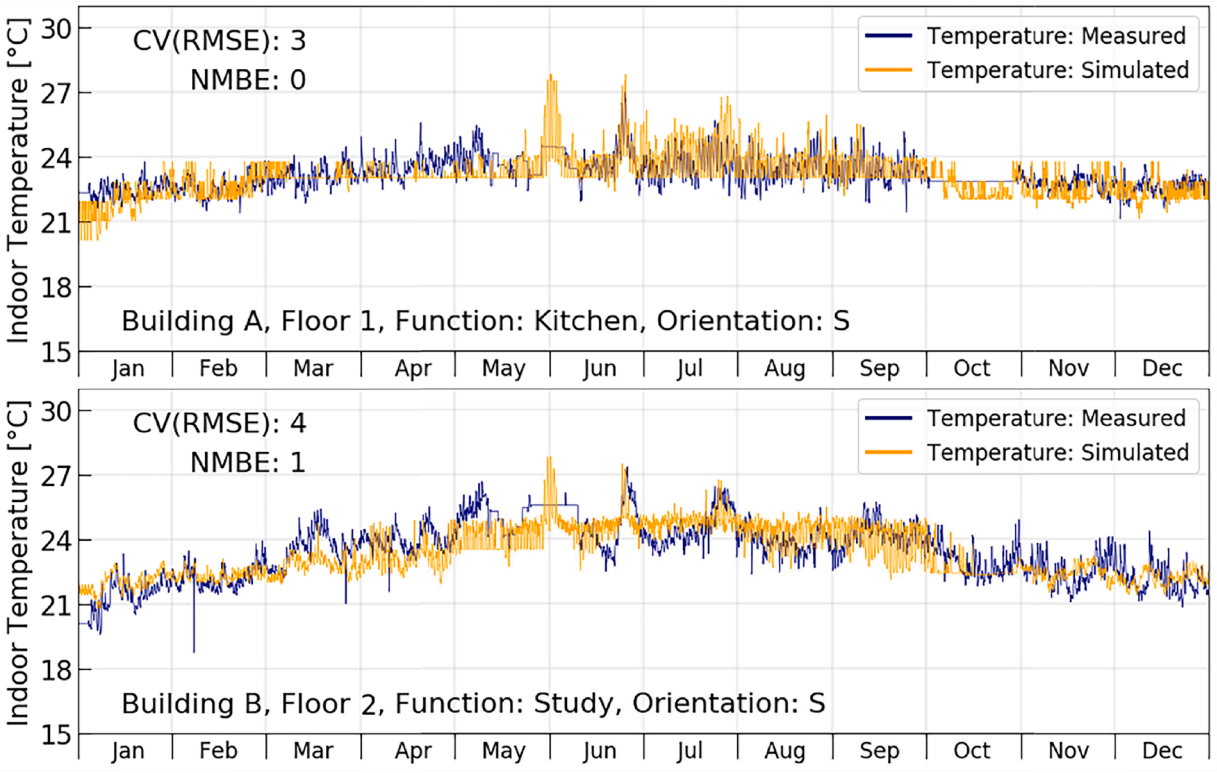

Fig. 8. Dry-bulb temperature for a southern kitchen in building A (top) and a southern study room in building B (bottom) as samples out of 63 zones. Measured values (dark blue) are compared against simulated data (orange).

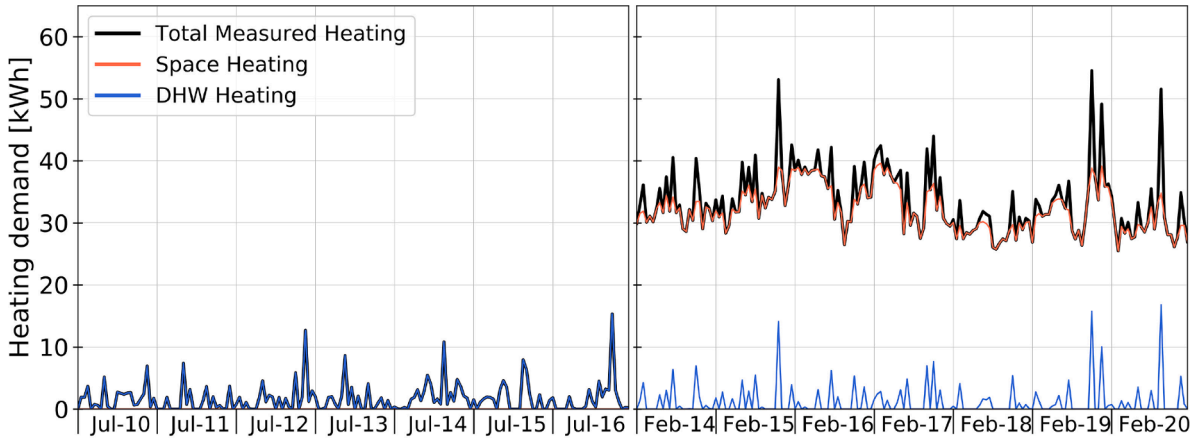

Fig. 9. DHW and SH separation from total measured heating demand for the one week with the lowest yearly demand, summer week (left), and the highest annual demand, winter week (right).

accumulated impacts of several continuous hours of high-temperature changes can be considered. The highest ΔT_d is around 3°C (average hourly temperature changes over 24 hours) for TDY and EWY. In TDY (green line), for three future periods, 51, 52, and 57 days have ΔT_d above 1°C (orange point), meaning that the temperature increase because of the effects of microclimate is more than 1°C per hour by average (yellow point) in those days, while 2, 3, and 8 days have ΔT_d larger than 2°C (2°C per hour by average). EWY also shows changes above 1°C for 85, 79, and 68 days and above 2°C during 11, 9, and 18 days over three periods. These numbers would significantly affect the degree-days values with increasing CDD and reducing HDD.

Degree-days are well-known in scientific communities as a metric to quantify the alteration in outdoor air temperature. Degree-days are simply related to the building energy demand. Many studies used CDD and HDD to assess the effects of UHI and climate change. In this research, due to the high-accuracy BEM, the results of EPS are used, which is more comprehensive and precise. However, to present a familiar metric, CDD and HDD are calculated and discussed in this section with a base temperature of 18°C. The calculated CDD and HDD for mesoclimate and microclimate TDY, EWY, and ECY over three future periods and the relative differences (RD (%)) are denoted in Table 8. In typical climate conditions (TDY) over three future periods, microclimate shows around 4% reduction in HDD, while CDD rises sharply by an average of 16%, which causes higher cooling loads. However, these changes are not proportional to the EPS result, presented later in this chapter, due to the consideration of solar gains and wind in EPS in addition to the air temperature.

CDD and HDD for each future period under microclimate conditions

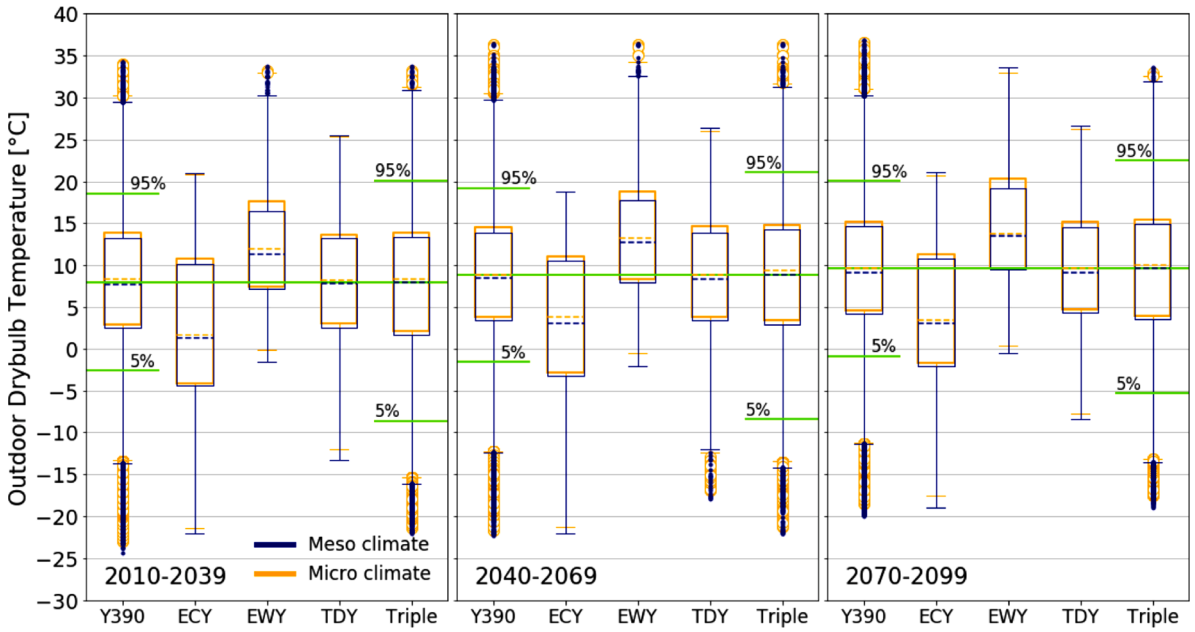

Fig. 10. Comparison of synthesized mesoclimate (dark blue) weather data with their corresponding microclimate (orange) for 13 scenarios for three periods. Y390 stands for thirteen 30-year scenarios, containing (13 × 30) × 8760 data points. ECY, EWY, and TDY are representative years (one year each), and Triple contains all three representatives (3 × 8760 data points). The short green lines show the 5th and 95th percentiles for Y390 and Triple. The median value of Triple is also marked in the graph (long green line) to be comparable with all boxes.

Table 7
Distribution and comparison of microclimate and mesoclimate for the representative future weather data.

		2010-2039			2040-2069			2070-2099		
		Meso[°C]	Micro[°C]	Diff.[°C]	Meso[°C]	Micro[°C]	Diff.[°C]	Meso[°C]	Micro[°C]	Diff.[°C]
TDY	mean	7.9	8.3	0.4	8.6	9.0	0.4	9.4	9.9	0.5
	5%	-2.6	-2.2	0.4	-1.6	-1.5	0.1	-0.9	-0.5	0.4
	50%	7.8	8.2	0.4	8.4	8.9	0.5	9.1	9.6	0.5
	95%	18.5	18.8	0.3	19.3	19.6	0.3	20.0	20.3	0.3
EWY	mean	12.1	12.7	0.6	13.3	13.9	0.6	14.5	15.0	0.5
	5%	2.9	3.4	0.5	3.9	4.5	0.6	5.7	6.1	0.4
	50%	11.3	12.0	0.7	12.7	13.3	0.6	13.5	13.8	0.3
	95%	23.9	24.3	0.4	24.5	25.1	0.6	25.7	26.2	0.5
ECY	mean	1.8	2.4	0.6	2.8	3.3	0.5	3.6	4.1	0.5
	5%	-14.5	-13.8	0.7	-13.0	-12.5	0.5	-10.2	-9.8	0.4
	50%	1.3	1.7	0.4	3.1	3.9	0.8	3.0	3.5	0.5
	95%	15.1	15.3	0.2	15.4	15.6	0.2	15.8	16.0	0.2

(Micro. Columns in Table 8) are depicted in Fig. 15, where each point shows the total degree-day and the line between each point shows the difference between periods. Accordingly, CDD shows 49% and 41% RD for the second and third periods, compared to the previous period. While HDD indicate 7% and 8% reduction over each period. EWY shows the highest RD in both CDD (increase) and HDD (decrease). Climate change has no considerable effect on CDD in ECY, while it influences HDD by 6% and 5% reduction during future periods in ECY.

Fig. 16 illustrates CDD for summer (July) and HDD for winter (February) over three future periods. CDD for EWY in July shows significantly larger values than TDY; around 500% larger on average. HDD for ECY in February is approximately 150% higher than TDY on average, over all the three time periods.

3.3. Energy performance simulations

3.3.1. Past conditions calibrated model

The first part of EPS results is related to the past condition. The annual hourly profiles of the measured and simulated (calibrated) SH demand for both buildings are presented in Fig. 17. The total heating demand for SH is equal to 142,200 kWh from measurements (DHW is excluded) and 138,000kWh from simulation (using measured weather data).

The second part of EPS results are correlated to future conditions and is analyzed in annual (long period) and weekly (short period) hourly profiles.

3.3.2. Future annual heating and cooling demand analysis

EPS results for three 30-year periods for 13 climate scenarios, introduced in section2.3, are presented in Fig. 18 (grey lines), where each period represents 390 years of simulations (13 scenarios). TDY is shown in the first row (green line), with reduced annual heating demands for 2040-2069 and 2070-2099 by 6% and 14%, respectively, compared to 2010-2039. EWY (red line) and ECY (blue line) are presented in the following graphs. EWY and ECY decline by 10% and 8% in the second period and 23% and 15% during the third period, respectively. As expected, heating demand falls every period due to the increasing temperature based on Table 7 and Fig. 10. According to the definition of the utilized representative weather data set, EWY and ECY are pessimistic future scenarios accumulating extreme warm and cold months, respectively. The probability of having such extreme years is relatively low, but they can show the bounds of the possible demands to

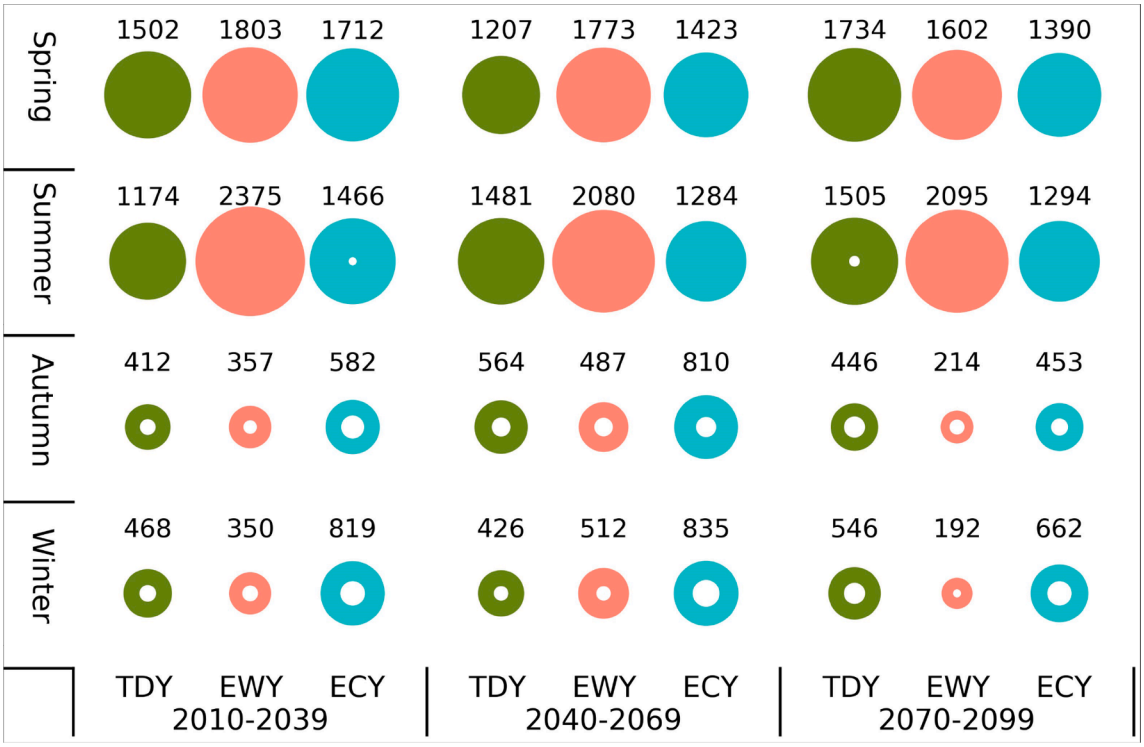

Fig. 11. Outdoor temperature differences between microclimate and mesoclimate ΔT for TDY (green), EWY (red), and ECY (blue) divided into four seasons over three future periods. Values on each bulb represent the summation of the season's hourly temperature difference (ΔT (°C)). The white area shows diurnal ΔT (°C).

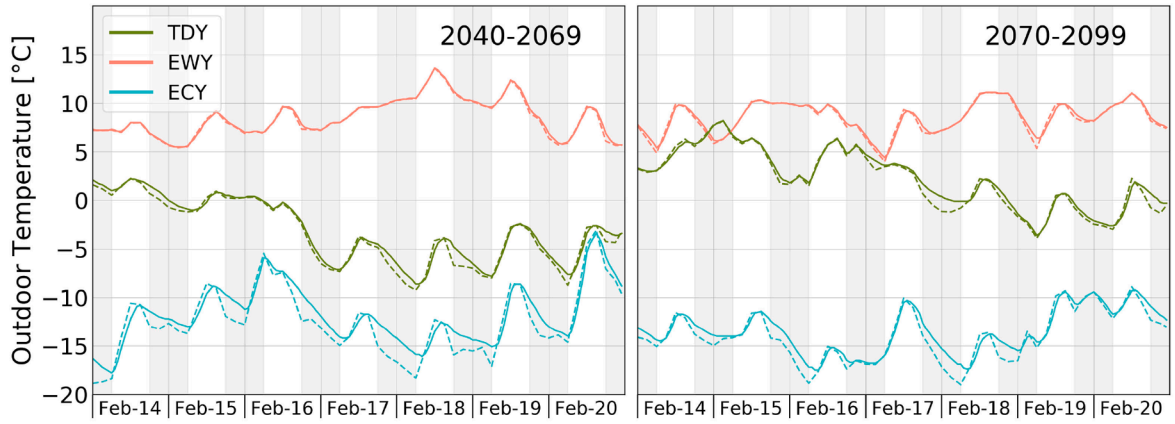

Fig. 12. Winter week outdoor dry-bulb temperature microclimate (solid line) and mesoclimate (dashed line) comparison for TDY (green), EWY (red), and ECY (blue) for the middle and end of the century. The grey zones show the nighttime (18:00 to 06:00).

assess the impacts of climate change and extreme conditions.

Cooling demands for building A over three 30-year periods (grey lines) are presented in Fig. 19. The first row of graphs shows TDY (green line), which rises significantly by four times for 2040-2069 and five times for 2070-2099. This growth happens in limited hours with high peak loads. The annual cooling demand shows a growth of 4.5 and 5.1 times in TDY for the second and third periods, respectively, while cooling peak loads grow by 210% and 290% over the second and third periods relative to 2010-2039 in EWY. For ECY, cooling demand is negligible, and naturally, there will not be any need for cooling during summertime in an extreme cold year in Sweden. Further study is done without the cooling system on building B to assess the impacts of higher outdoor temperature on indoor thermal comfort, discussed in the following section.

Cumulative summaries of heating and cooling demand are shown in Fig. 20. Following the same pattern as before, 390 years of simulations (grey lines) are enveloped by EWY (red line) at the lower bound and ECY (blue line) at the higher bound, while TDY (green line) is stretched in the middle. Cooling demand has an opposite arrangement. The substantial differences between the EWY and ECY with TDY and 390 years are due to the aggregated pessimistic situation in the extreme scenarios; hence extreme conditions are used mostly for short period analysis. Dramatic growth in cooling demand can be seen in the second row of the graphs. In 2040-2069 the cooling system starts to work from mid-June, while the cooling device starts to work one month earlier in 2070-2099, due to the longer warm season.

3.4. Future weekly heating and cooling demand analysis

An enlarged graph for hourly demand for the summer week is presented in Fig. 21. Cooling demand for 150 years of simulation (five GCMs) for RCP 8.5 (grey lines) is shown against EWY (red line) for 2070-

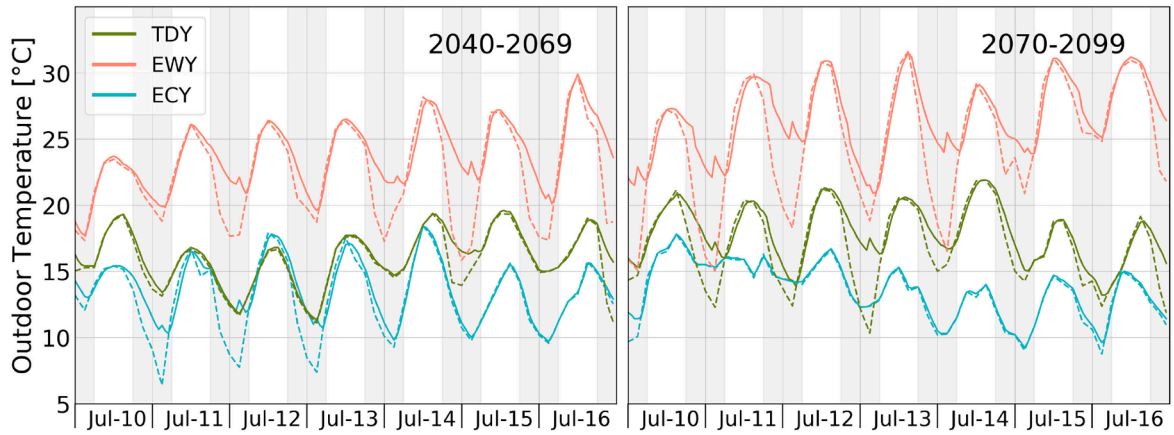

Fig. 13. Summer week outdoor dry-bulb temperature microclimate (solid line) and mesoclimate (dashed line) comparison for TDY (green), EWY (red), and ECY (blue) for the middle and end of the century. The grey zones show the nighttime (18:00 to 06:00).

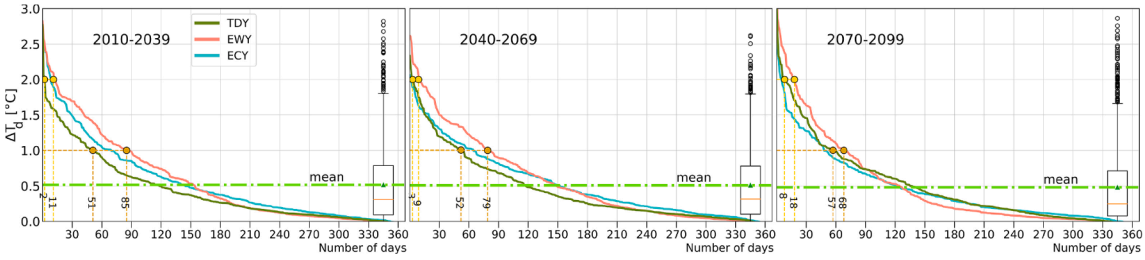

Fig. 14. Duration diagram for daily outdoor temperature differences (ΔT_d (°C)) between microclimate and mesoclimate for TDY (green), EWY (red), and ECY (blue) over three future periods.

Table 8
CDD and HDD for mesoclimate and microclimate representative weather data and comparison with the relative difference (RD) over three 30-year future periods.

		2010-2039			2040-2069			2070-2099		
		Meso.[°C]	Micro.[°C]	RD[%]	Meso[°C]	Micro[°C]	RD[%]	Meso[°C]	Micro[°C]	RD[%]
CDD	TDY	42	49	14%	61	74	18%	87	104	16%
	EWY	280	332	16%	363	442	18%	492	590	17%
	ECY	2	2	0%	1	1	0%	3	3	0%
HDD	TDY	3742	3590	-4%	3501	3351	-4%	3240	3075	-5%
	EWY	2428	2270	-7%	2086	1958	-7%	1788	1704	-5%
	ECY	5904	5704	-4%	5561	5370	-4%	5246	5080	-3%

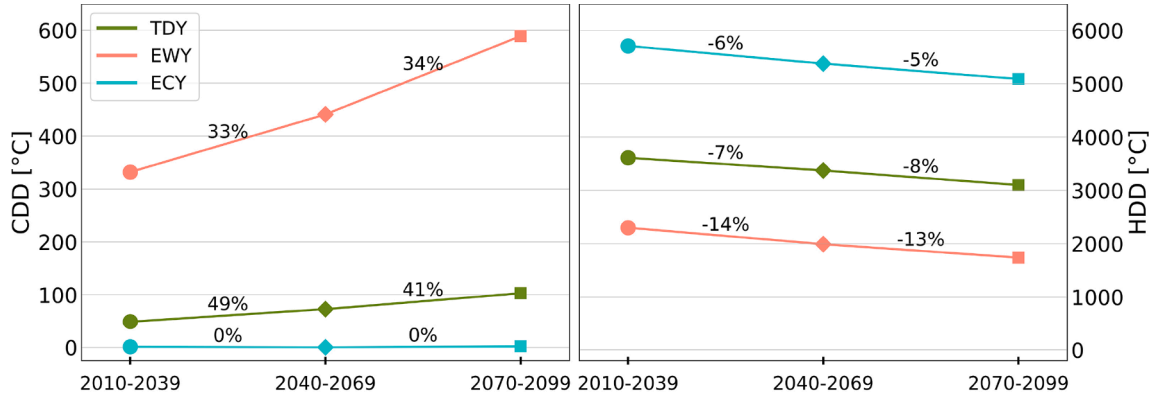

Fig. 15. CDD (left) and HDD (right) for the beginning (circle), middle (diamond), and end (square) of the century. RDs [%] are denoted over each period.

2099, which is, perhaps, one of the worst conditions regarding the high temperature due to the climate change, showing adequately the climate change impacts on the cooling load for an extreme warm scenario. While the annual cooling demand rises by 23%, the microclimate EPS for EWY (solid red line) depicts 4% growth in the cooling peak power (yellow circle) compared to mesoclimate EWY (dashed red line). Meanwhile, the

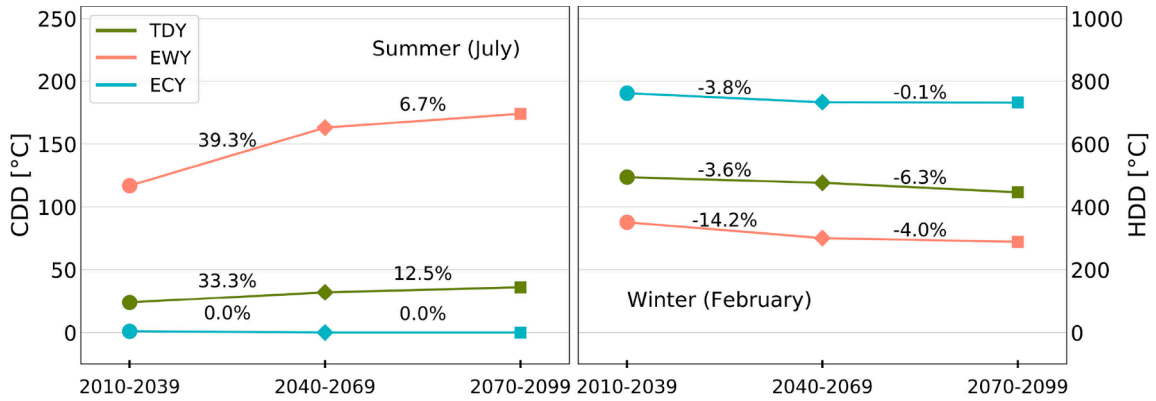

Fig. 16. CDD in summer (left) and HDD in winter (right) for the beginning (circle), middle (diamond), and end (square) of the century. RDs [%] are denoted over each period.

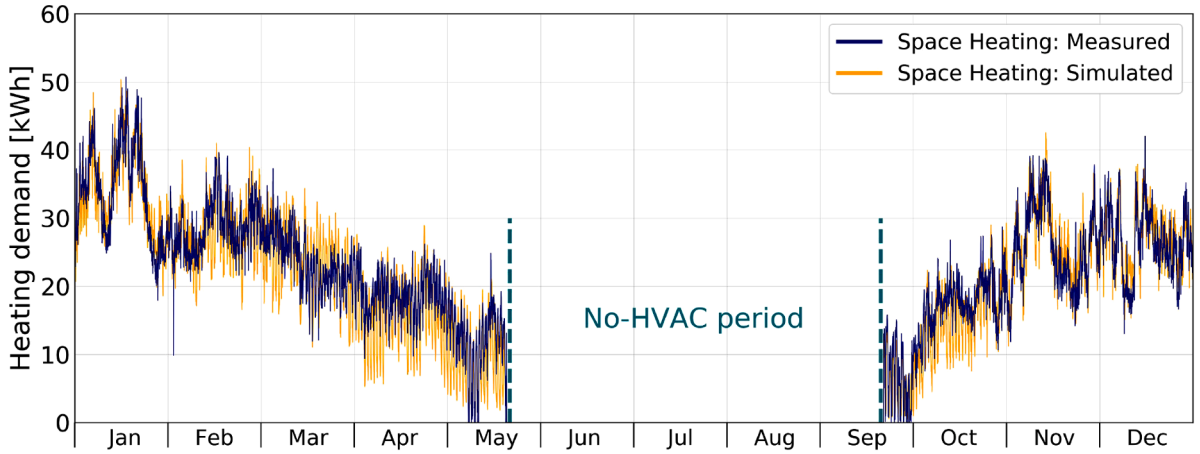

Fig. 17. Hourly measured values (dark blue) for SH against simulation results (orange).

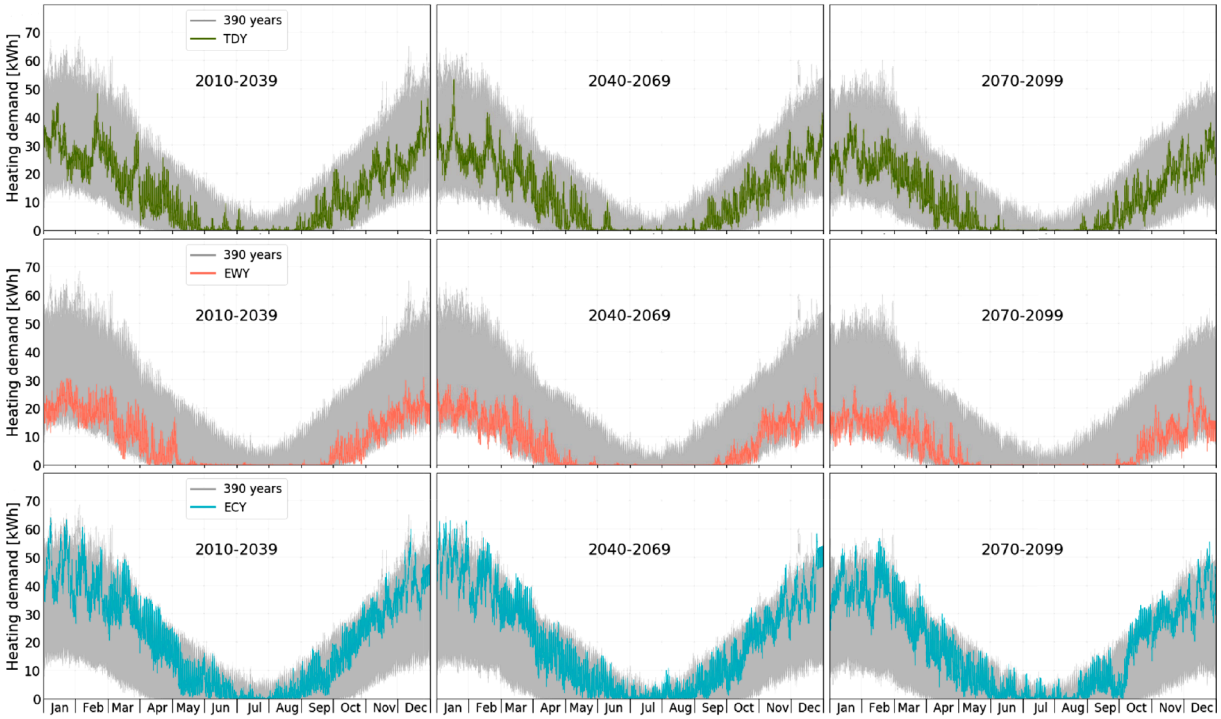

Fig. 18. Hourly profile of heating demand for 390 years (13 climate scenarios) of simulations and TDY (top), EWY (middle), and ECY (bottom).

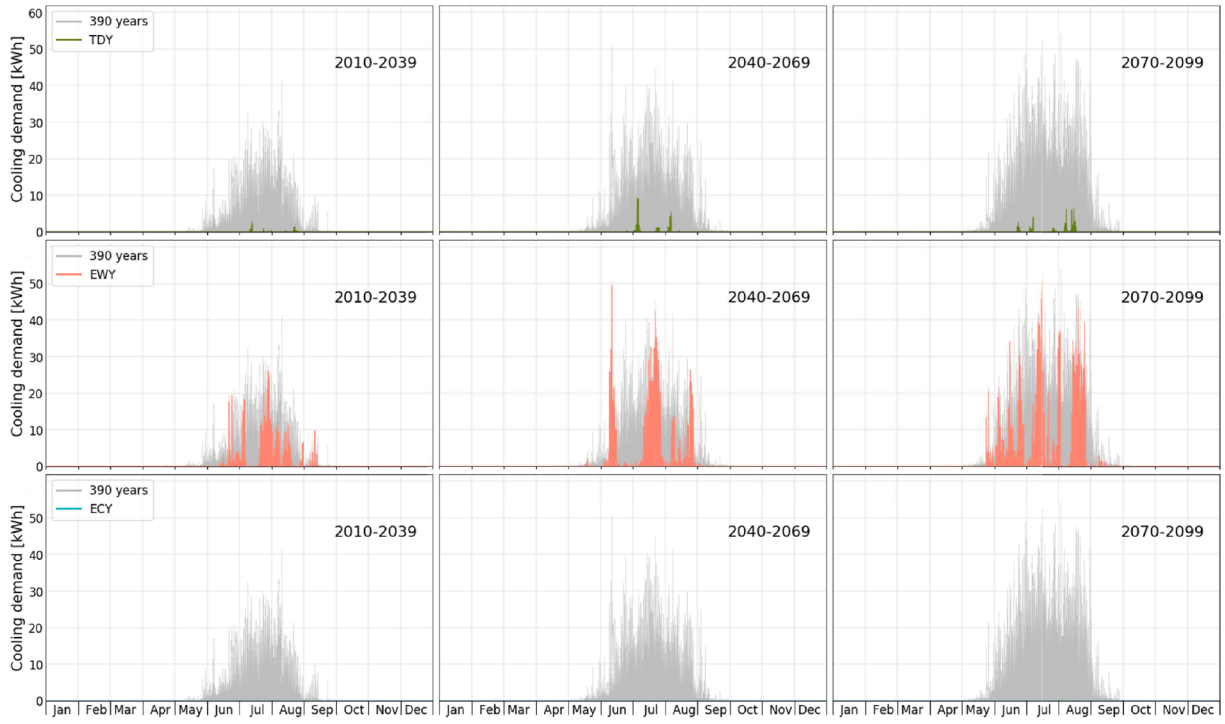

Fig. 19. Hourly profile of cooling demand for 390 years (13 climate scenarios) of simulations and TDY (top), EWY (middle), and ECY (bottom).

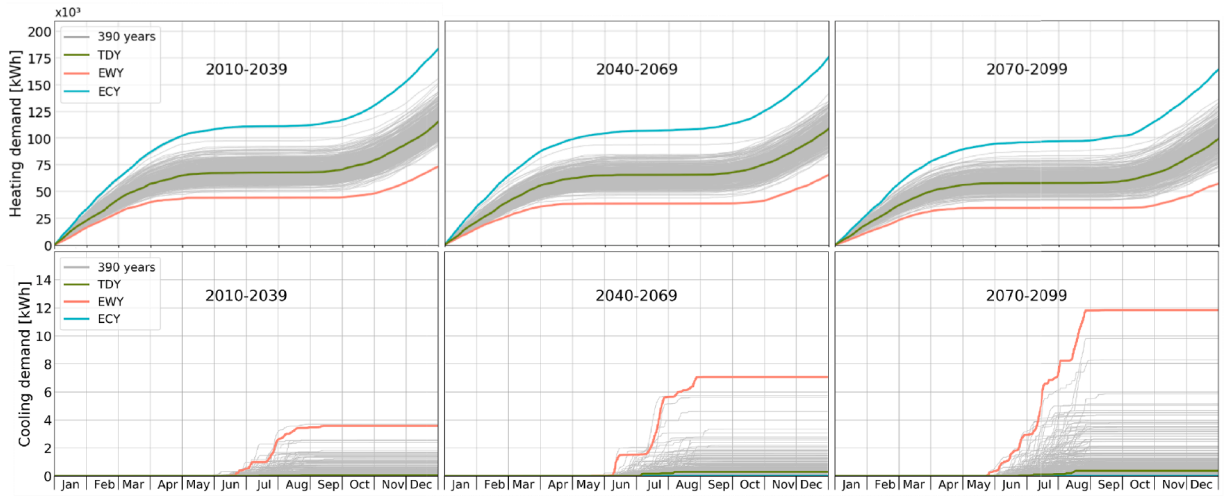

Fig. 20. Cumulative summary of heating (top) and cooling demand (bottom) for 390 years simulation (grey), TDY (green), EWY (red), and ECY (blue).

daily peak loads are increased up to 25% under the effects of microclimate conditions and UHI; for instance, July 10th, 11th, and 14th have a rise in peak load by 25%, 16%, and 13% (blue circles).

Magnified hourly heating demand for the winter week is illustrated in Fig. 22. Heating demand for 150 years of simulation (five GCMs) for RCP 4.5 (grey lines) is shown against ECY (blue line) for 2040-2079. The microclimate conditions (solid blue line) shows a 3% reduction in the peak load and 4% in the annual demand compared to the mesoclimate conditions (dashed blue line). In the winter week, daily demand reduces by an average of 5%. As discussed in section 3.2, the effects of UHI in winter is not as significant as in summer, which appears in the lower changes in the heating demand, considering the fact that this change is desired.

3.4.1. *Future indoor thermal comfort analysis*

To assess the impacts of future weather on indoor comfort, building B was simulated without the cooling system. In this case, the reference point for overheating is defined at 26°C. The first row of graphs in Fig. 23 represents TDY (green line) for three periods of 30-year. For the second period, TDY has 67 hours above 26°C and 96 hours for the last period. EWY (red line) shows an enormous number of overheating hours by 1180 and 1630 for 2040-2069 and 2070-2099, respectively. Moreover, during the warm season, from June 01 to September 30, average temperatures are 25.9°C, 26.7°C, and 27.4°C with standard deviations of 1.7, 2.1, and 2.1 for the three periods. Accordingly, the number of overheating hours is significant. Moreover, the hourly temperature has a higher range with spikes over 32°C. ECY (blue line) has no overheating during the future periods. Overheating hours in 390 years of simulations have an average of 73 for 2040-2069 and 133 for 2070-2099; these

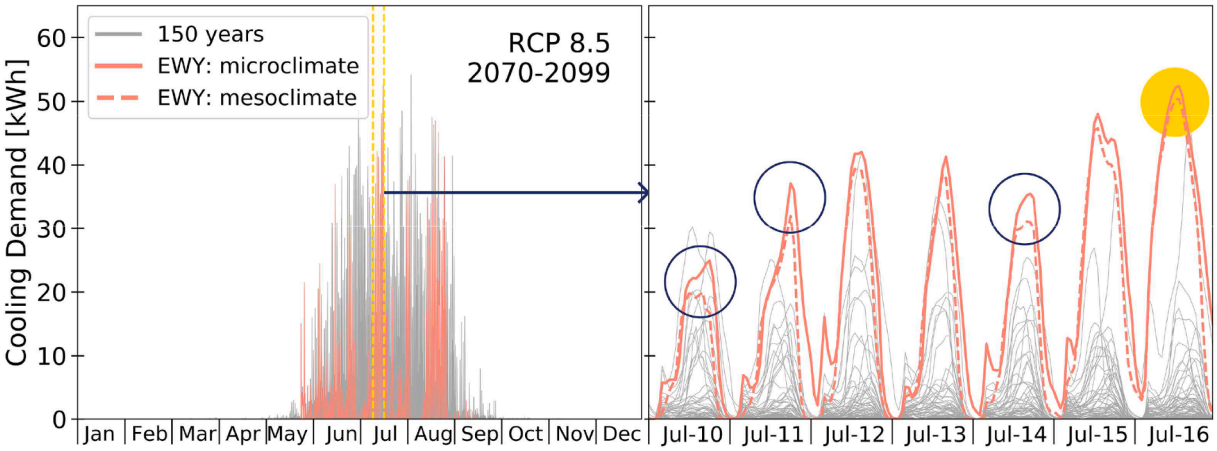

Fig. 21. Annual (left) and enlarged section of hourly cooling demand for the summer week (right) for 150 years simulations RCP 8.5 (grey), EWY microclimate (solid red), and EWY mesoclimate (dashed red) for 2070-2099.

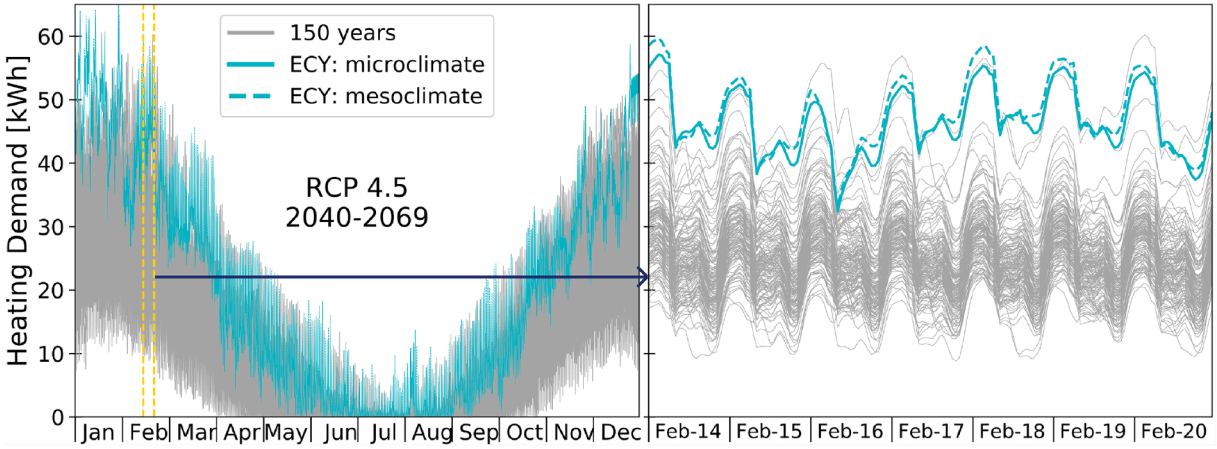

Fig. 22. Annual (left) and enlarged section of hourly heating demand for the sample week in winter (right) for 150 years simulations for RCP 4.5 (grey), and ECY microclimate (yellow), and ECY mesoclimate (red) for 2040-2069.

numbers are influenced and reduced by RCP 2.6. Particularly RCP 8.5 has an average of 98 and 232 hours for the second and third periods, which is considerable.

Enlarged views of the hourly profile of the summer week indoor temperatures are illustrated in Fig. 24. The indoor temperature in EWY (red line) remains above 26°C continuously for several days, especially in 2070-2099, while it is lower only for a few hours before sunrise over 2040-2069. In addition, overheating occurs in several different years for RCP 8.5 (grey lines) continuously in a day, significantly affecting thermal comfort in that particular time, even though they do not represent the warmest year. Furthermore, natural ventilation through opening the windows was activated above the indoor temperature of 24°C; however, it is not sufficient for diurnal hours (white zones) in 2040-2069, and it is not adequate even for nocturnal hours (grey zones) over the last period. Nevertheless, the effect of natural ventilation is noticeable in TDY (green line) as the outdoor air is sufficient to cool down interior space, and the summits of the curves are flattened.

Comparison between indoor temperature for mesoclimate and microclimate EPS in the summer week shows a significant difference in indoor temperature, especially at nocturnal hours (grey zones). The temperature difference of up to 3°C for several days can be seen in Fig. 25. The mesoclimate EPS results (dashed line), commonly applied in EPSs, mostly show temperatures below the yellow line at night, which eliminates the thermal discomfort conditions in the assessments. The high indoor temperature leads to higher thermal discomfort, where most of the occupancy hours in residential buildings happen at night. Also, it will eliminate the effect of night flush to reduce the overheating for the coming day. This situation should be considered by urban energy providers to avoid power outages since happening EWY conditions for a week is quite possible. Some statistics for indoor temperature under mesoclimate and microclimate are presented in Table 9.

The effects of extreme conditions are investigated on the HVAC system. Fig. 26 illustrates the working hours for the heating and cooling system. Each line represents one hour on or off for the system, and their color gradient shows the power intensity. The heating system always works during the five months of November, December, January, February, and March for ECY and TDY. ECY induces higher heating powers than TDY in all three periods (darker colors) for about two months. The cooling load shows a significant difference between TDY and EWY. The cooling system is active in 190, 410, and 530 hours for the three periods in TDY, while for EWY, it works 1320, 1530, and 1860 hours with higher intensities. Also, the cooling system is continuously required for EWY over 2040-2069 and 2070-2099 for almost three months during June, July, and August. This analysis can provide energy suppliers with a realistic demand curve to avoid power blackout with an accurate forecast.

4. Conclusion

This research investigated the impacts of climate change and

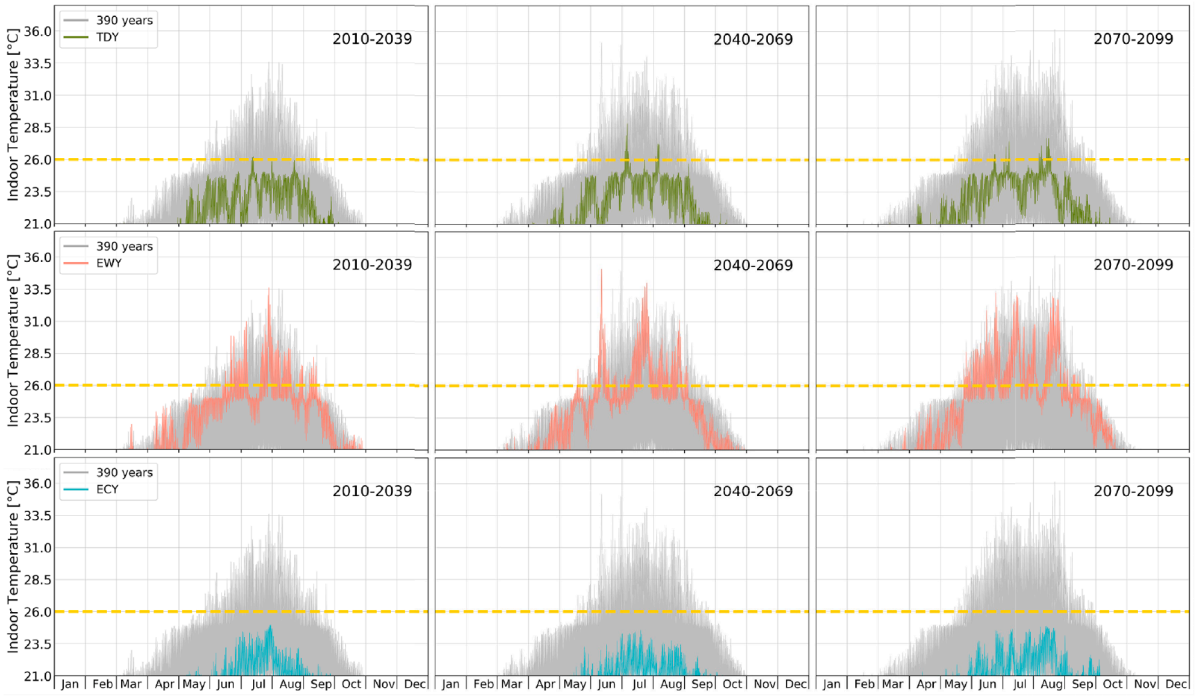

Fig. 23. Indoor dry-bulb temperature for building B without the cooling system for 390 years simulations (grey) for every 30-year period, TDY (top), EWY (middle), and ECY (bottom). The yellow dashed line delineates 26°C for the overheating reference point.

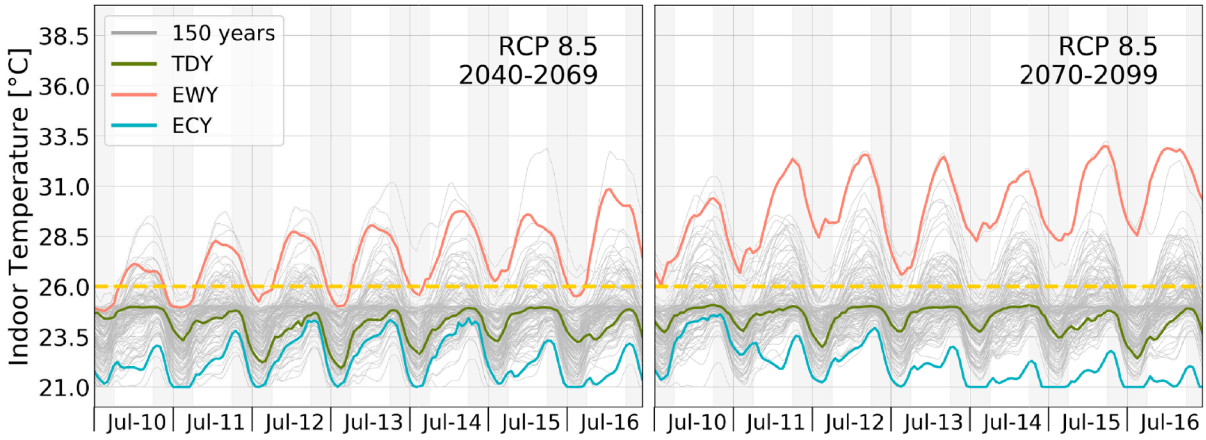

Fig. 24. Enlarged hourly indoor dry-bulb temperature for summer sample week for 150 years simulations for RCP 8.5 (grey), TDY (green), EWY (red), and ECY (blue) for 2040-2069 (left) and 2070-2099 (right). The grey zones show the nighttime (18:00 to 06:00). All data are for microclimate conditions.

extreme weather on the energy performance and indoor thermal comfort of buildings, considering microclimate effects. The analysis was performed for two multi-family buildings in Southeastern Sweden and adopted high spatiotemporal resolution data, including measured data on heating energy demand, indoor thermal condition and outdoor temperature. The measured heating demand included space heating and domestic hot water; therefore, a non-parametric method was applied to separate their hourly values from the total demand. The research workflow was divided into past and future climate conditions, where historical and monitored weather data were used as well as the measured heating demand and indoor temperature to calibrate and verify the building energy model for the past conditions. The future conditions were studied by simulating the verified BEM using RCM future climate data and considering 13 different future climate scenarios. Three sets of representative weather data sets were synthesized for three 30-year future periods, consisting of TDY, EWY, and ECY. This collection of future weather data enabled us to conduct a comprehensive assessment, considering a wide range of possible future conditions, climate uncertainties, and typical and extreme weather conditions. By simulating the microclimate conditions for the future representative weather data sets, we could investigate the impacts of microclimate on the energy performance of buildings during typical and extreme weather conditions in addition to the climate change impacts over three future periods.

According to the results, the mesoclimate conditions for TDY had the annual average temperature of 7.9°C, 8.6°C, and 9.4°C, over three future periods (2010-2039, 2040-2069, and 2070-2099), while the corresponding microclimate had an average of 8.3°C (+5%), 9.0°C (+4%), and 9.9°C (+5%), respectively. Dividing the outdoor temperature results for microclimate conditions into daytime (06:00-18:00) and nighttime (18:00-06:00) helped to better understand the impacts of urban morphology on microclimate. Apparently, the increase mostly occurs at

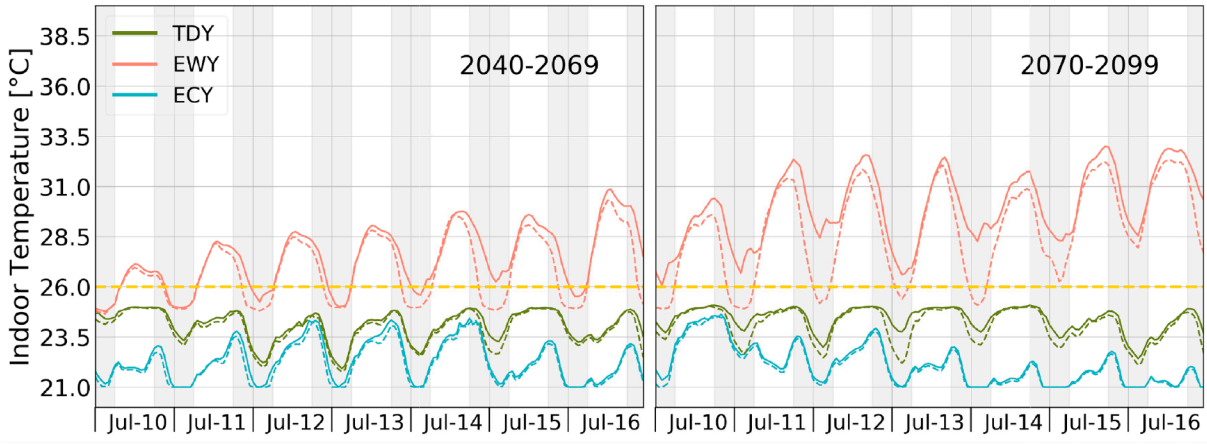

Fig. 25. Indoor temperature for microclimate (solid lines) against mesoclimate (dashed lines) for the second and third periods. TDY (green), EWY (red), and ECY (blue) are compared against the 26°C (dashed yellow) mark line. The grey zones show the nighttime (18:00 to 06:00).

Table 9
5th, 50th, and 95th percentile for indoor temperature over the three future periods from EPS with microclimate and mesoclimate conditions in three representative weather scenarios.

		2010-2039			2040-2069			2070-2099		
		Meso[°C]	Micro[°C]	Diff.[°C]	Meso[°C]	Micro[°C]	Diff.[°C]	Meso[°C]	Micro[°C]	Diff.[°C]
TDY	mean	21.6	21.7	0.1	21.8	21.9	0.1	21.9	22.0	0.1
	5%	21.0	21.0	0.0	21.0	21.0	0.0	21.0	21.0	0.0
	50%	21.0	21.0	0.0	21.0	21.0	0.0	21.0	21.0	0.0
	95%	24.4	24.6	0.2	24.8	24.9	0.1	24.9	25.0	0.1
EWY	mean	22.5	22.7	0.2	22.8	22.9	0.1	23.1	23.2	0.1
	5%	21.0	21.0	0.0	21.0	21.0	0.0	21.0	21.0	0.0
	50%	21.0	21.0	0.0	21.0	21.0	0.0	21.0	21.1	0.1
	95%	26.9	28.4	1.5	27.6	28.4	0.8	28.4	29.2	0.8
ECY	mean	21.2	21.2	0.0	21.2	21.2	0.0	21.3	21.3	0.0
	5%	21.0	21.0	0.0	21.0	21.0	0.0	21.0	21.0	0.0
	50%	21.0	21.0	0.0	21.0	21.0	0.0	21.0	21.0	0.0
	95%	22.6	22.8	0.2	22.4	22.6	0.2	23.1	23.3	0.2

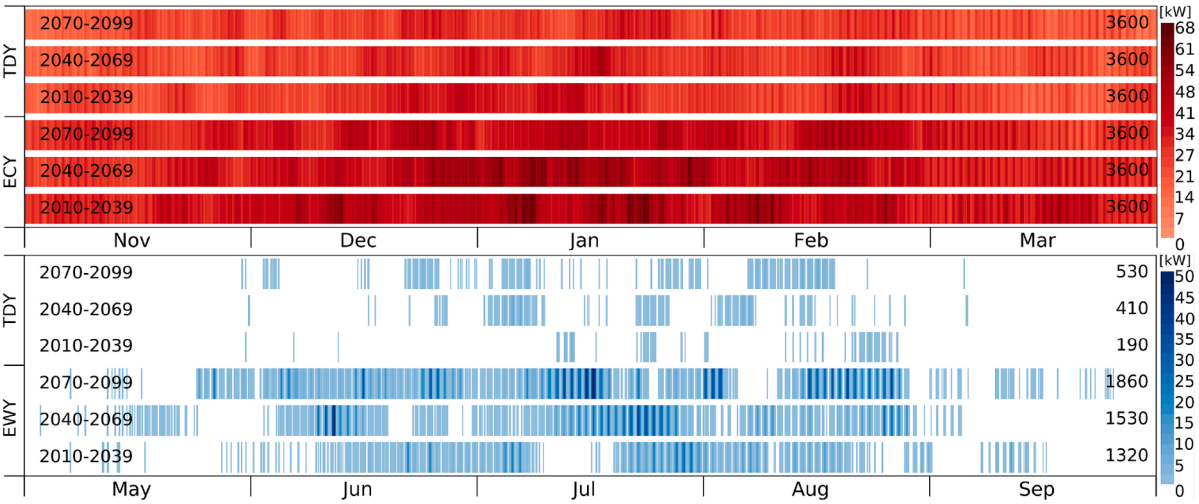

Fig. 26. Heating system (Top) working hours for TDY against ECY in winter, and cooling system (Bottom) working hours for TDY against EWY in summer. The color gradient shows the power intensity. Numbers on the right present the number of working hours, regardless of the intensity.

nighttime, having a total share of 95% and up to 10.6°C against 5.9°C during daytime. These cause thermal comfort disruption since the highest occupancy for residential buildings happens at night. Spring and summer showed the highest outdoor temperature change with 75% of the annual change, including both daytime and nighttime peaks. Moreover, degree-days (CDD and HDD) were calculated as well-known metrics for practitioners. Cooling degree-day increased by 16%, while heating degree-day reduced by 4% in TDY conditions directly affect the cooling and heating demand.

Considering the energy performance of buildings, a comparison

between energy demands for three future periods showed a reduction in heating demand by 6% in 2040-2069 and 14% in 2070-2099 related to 2010-2039 for typical weather conditions (TDY). On the other hand, cooling demands demonstrated significant growth of four and five times for the second and third periods under climate change impacts. Cooling peak loads climbed by 210% over 2040-2069 and 290% over 2070-2099 compared to 2010-2039 for TDY. Considering the fact that extreme weather events are not accounted in EPS with TMY weather file, energy demand and indoor thermal comfort were assessed in a high-resolution time step for extreme conditions. In an extreme warm week, the daily cooling peak load increased up to 25%. In a typical year (TDY) cooling system works for 190, 410, and 530 hours in 2010-2039, 2040-2069, and 2070-2099, respectively, while it works 1320 (+690%), 1530 (+370%), and 1860 (+350%) hours in an extreme warm year (EWY) over the future periods. This explains the significant role of cooling systems in the future to maintain thermal comfort and energy efficiency.

In the absence of cooling systems during an extreme warm year (EWY), natural ventilation was not sufficient to remove the heat from interior spaces and the average indoor temperature during the warm season were 25.9°C, 26.7°C, 27.4°C for three future periods with a maximum of 29°C, 30°C, and 32°C. This assessment showed that it is probable to have an indoor temperature above 26°C for almost one week continuously. These all indicate that not accounting for influencing climate variations can result in maladaptation or insufficient adaptation of urban areas to climate change. This can become very critical in Sweden, where residential buildings are mostly not equipped with cooling systems, inducing considerable health risks and/or cooling loads in the future. Therefore, further studies, especially with high spatio-temporal resolutions data and models, are needed to assess the tenants' well-being and energy demands during future extreme weather conditions.

Declaration of Competing Interest

None.

Acknowledgements

This work was supported by the joint programming initiative 'ERA-Net Smart Energy Systems' focus initiative on Integrated, Regional Energy Systems, with support from the European Union's Horizon 2020 research and innovation programme [775970] and the European Union's Horizon 2020 research and innovation programme under grant agreement for the COLLECTiEF (Collective Intelligence for Energy Flexibility) project (grant agreement ID: 101033683). Supports of the Centre for Innovation Research at Lund University (CIRCLE) and Sweden's innovation agency (VINNOVA - MIRAI) are acknowledged.

References

Amasyali, K., & El-Gohary, N. M. (2018). A review of data-driven building energy consumption prediction studies. *Renewable and Sustainable Energy Reviews, 81*, 1192–1205. https://doi.org/10.1016/j.rser.2017.04.095

ASHRAE Guideline 14. (2014). In —*Measurement of Energy, Demand, and Water Savings*. www.ashrae.org.

Bacher, P., de Saint-Aubain, P. A., Christiansen, L. E., & Madsen, H. (2016). Non-parametric method for separating domestic hot water heatingspikes and space heating. *Energy and Buildings, 130*, 107–112. https://doi.org/10.1016/j.enbuild.2016.08.037

Baker, P. (2011). Historic Scotland Technical Paper 10: U-values and traditional buildings In situ measurements and their comparisons to calculated values. *Glasgow Caledonian University*. www.historic-scotland.gov.uk/technicalpapers.

Battista, G., Roncone, M., & de Lieto Vollaro, E. (2021). Urban Overheating Impact: A Case Study on Building Energy Performance. *Applied Sciences, 11*(18), 8327. https://doi.org/10.3390/app11188327

Berardi, U., & Jafarpur, P. (2020). Assessing the impact of climate change on building heating and cooling energy demand in Canada. *Renewable and Sustainable Energy Reviews, 121*, Article 109681. https://doi.org/10.1016/j.rser.2019.109681

Bhandari, M., Shrestha, S., & New, J. (2012). Evaluation of weather datasets for building energy simulation. *Energy and Buildings, 49*, 109–118. https://doi.org/10.1016/j.enbuild.2012.01.033

Biljecki, F. (2017). *Level of detail in 3D city models*. https://doi.org/10.4233/uuid:f12931b7-5113-47ef-bfd4-688aae3be248.

Biljecki, F., Ledoux, H., & Stoter, J. (2016). *Generation of multi-LOD 3D city models in CityGML with the procedural modelling engine Random3Dcity. IV-4/W1*, 51–59. https://doi.org/10.5194/isprs-annals-IV-4-W1-51-2016.

Biswas, M. A. R., Robinson, M. D., & Fumo, N. (2016). Prediction of residential building energy consumption: A neural network approach. *Energy, 117*, 84–92. https://doi.org/10.1016/j.energy.2016.10.066

Bourisli, R. I., Altarakma, M. A., & AlAnzi, A. A. (2018). General correlation of building energy use via hybrid genetic programming/genetic algorithm. *Journal of Solar Energy Engineering, Transactions of the ASME, 140*(4), 00. https://doi.org/10.1115/1.4039447. Scopus.

Bueno, B., Hidalgo, J., Pigeon, G., Norford, L., & Masson, V. (2013). Calculation of Air Temperatures above the Urban Canopy Layer from Measurements at a Rural Operational Weather Station. *Journal of Applied Meteorology and Climatology, 52*(2), 472–483. https://doi.org/10.1175/JAMC-D-12-083.1

Bueno, B., Pigeon, G., Norford, L. K., Zibouche, K., & Marchadier, C. (2012). Development and evaluation of a building energy model integrated in the TEB scheme. *Geoscientific Model Development*, 5(2), 433–448. https://doi.org/10.5194/gmd-5-433-2012.

Bueno, B., Roth, M., Norford, L., & Li, R. (2014). Computationally efficient prediction of canopy level urban air temperature at the neighbourhood scale. *Urban Climate, 9*, 35–53. https://doi.org/10.1016/j.uclim.2014.05.005. Scopus.

Burman, E., & Mumovic, D. (2017). Measurement and Verification Models for Cost-Effective Energy-Efficient Retrofitting. In *Cost-Effective Energy Efficient Building Retrofitting—1st Edition*. Elsevier. https://www.elsevier.com/books/cost-effective-energy-efficient-building-retrofitting/pacheco-torgal/978-0-08-101128-7.

Campbell, R. J. (2013). *Weather-related power outages and electric system resiliency*. 103–118.

Chen, Y., Moufouma-Okia, W., Masson-Delmotte, V., Zhai, P., & Pirani, A. (2018). Recent Progress and Emerging Topics on Weather and Climate Extremes Since the Fifth Assessment Report of the Intergovernmental Panel on Climate Change. *Annual Review of Environment and Resources, 43*(1), 35–59. https://doi.org/10.1146/annurev-environ-102017-030052

Crawley, D. (1998). Which Weather Data Should You Use for Energy Simulations of Commercial Buildings? *ASHRAE Transactions, 104*, 498–515.

Crawley, D., Hand, J. W., Kummert, M., & Griffith, B. T. (2008). Contrasting the capabilities of building energy performance simulation programs. *Building and Environment, 43*(4), 661–673. https://doi.org/10.1016/j.buildenv.2006.10.027

Cronin, J., Anandarajah, G., & Dessens, O. (2018). Climate change impacts on the energy system: A review of trends and gaps. *Climatic Change, 151*(2), 79–93. https://doi.org/10.1007/s10584-018-2265-4

Cui, Y., Yan, D., Hong, T., Xiao, C., Luo, X., & Zhang, Q. (2017). Comparison of typical year and multiyear building simulations using a 55-year actual weather data set from China. *Applied Energy, 195*, 890–904. https://doi.org/10.1016/j.apenergy.2017.03.113

Deb, C., Zhang, F., Yang, J., Lee, S. E., & Shah, K. W. (2017). A review on time series forecasting techniques for building energy consumption. *Renewable and Sustainable Energy Reviews, 74*, 902–924. https://doi.org/10.1016/j.rser.2017.02.085

Ding, Y., Shen, Y., Wang, J., & Shi, X. (2015). *Uncertainty sources and calculation approaches for building energy simulation models*. 78, 2566–2571. Scopus. https://doi.org/10.1016/j.egypro.2015.11.283.

Ellis, P., & Torcellini, P. (2005). *Simulating Tall Buildings Using EnergyPlus: Preprint*.

EnergyPlus. (2021). Weather Data for Simulation | EnergyPlus. https://energyplus.net/weather/simulation.

Erba, S., Causone, F., & Armani, R. (2017). The effect of weather datasets on building energy simulation outputs. *Energy Procedia, 134*, 545–554. https://doi.org/10.1016/j.egypro.2017.09.561

Fan, C., Yan, D., Xiao, F., Li, A., An, J., & Kang, X. (2021). Advanced data analytics for enhancing building performances: From data-driven to big data-driven approaches. *Building Simulation, 14*(1), 3–24. https://doi.org/10.1007/s12273-020-0723-1

FEBY. (2019). *Kravspecifikation för energieffektiva byggnader Bostäder och lokaler*. FEBY (Forum för Energieffektivt Byggande). https://www.feby.se/files/rapporter/2019-12-12-kravspecifikation-feby18.pdf.

FEMP. (2015). *M&V Guidelines: Measurement and Verification for Performance-Based Contracts (Version 4.0)*. The US Department of Energy Federal Energy Management Program. https://www.energy.gov/eere/femp/downloads/mv-guidelines-measurement-and-verification-performance-based-contracts-version.

Gao, Y., Zhao, J., & Han, L. (2022). Exploring the spatial heterogeneity of urban heat island effect and its relationship to block morphology with the geographically weighted regression model. *Sustainable Cities and Society, 76*. Scopus. https://doi.org/10.1016/j.scs.2021.103431.

Gasparrini, A., Guo, Y., Hashizume, M., Lavigne, E., Zanobetti, A., Schwartz, J., Tobias, A., Tong, S., Rocklöv, J., Forsberg, B., Leone, M., Sario, M. D., Bell, M. L., Guo, Y.-L. L., Wu, C., Kan, H., Yi, S.-M., Coelho, M., de Sousa Zanotti Stagliorio Coelho, M, Saldiva, P. H. N., … Armstrong, B. (2015). Mortality risk attributable to high and low ambient temperature: A multicountry observational study. *The Lancet, 386*(9991), 369–375. https://doi.org/10.1016/S0140-6736(14)62114-0

Good, P., Gregory, J., Lowe, J., & Andrews, T. (2012). Abrupt CO2 experiments as tools for predicting and understanding CMIP5 representative concentration pathway scenarios. *Climate Dynamics, 40*, 00. https://doi.org/10.1007/s00382-012-1410-4

Goy, S., Maréchal, F., & Finn, D. (2020). Data for Urban Scale Building Energy Modelling: Assessing Impacts and Overcoming Availability Challenges. *Energies, 13*(16), 4244. https://doi.org/10.3390/en13164244

Huang, P., Huang, G., & Wang, Y. (2015). HVAC system design under peak load prediction uncertainty using multiple-criterion decision making technique. *Energy and Buildings, 91*, 26–36. https://doi.org/10.1016/j.enbuild.2015.01.026. Scopus.

Huang, Y., & Li, C. (2021). Accurate heating, ventilation and air conditioning system load prediction for residential buildings using improved ant colony optimization and wavelet neural network. *Journal of Building Engineering, 35*, 00. https://doi.org/10.1016/j.jobe.2020.101972. Scopus.

Hulme, J., & Doran, S. (2014). *In-situ measurements of wall U-values in English housing* (No. 290–102; p. 82). Department of Energy and Climate Change. https://assets.publishing.service.gov.uk/government/uploads/system/uploads/attachment_data/file/409428/In-situ_u-values_final_report.pdf.

Ioannou, A., & Itard, L. C. M. (2015). Energy performance and comfort in residential buildings: Sensitivity for building parameters and occupancy. *Energy and Buildings, 92*, 216–233. https://doi.org/10.1016/j.enbuild.2015.01.055

Janjai, S., & Deeyai, P. (2009). Comparison of methods for generating typical meteorological year using meteorological data from a tropical environment. *Applied Energy, 86*(4), 528–537. https://doi.org/10.1016/j.apenergy.2008.08.008. Scopus.

Javanroodi, K. (2018). *Wind-phil Architecture: Optimization of high-rise buildings form for efficient summer cooling in Tehran*. Tarbiat Modares University.

Javanroodi, K., Mahdavinejad, M., & Nik, V. M. (2018). Impacts of urban morphology on reducing cooling load and increasing ventilation potential in hot-arid climate. *Applied Energy, 231*, 714–746. https://doi.org/10.1016/j.apenergy.2018.09.116. Scopus.

Javanroodi, K., & Nik, V. (2019). Impacts of Microclimate Conditions on the Energy Performance of Buildings in Urban Areas. *Buildings, 9*, 00. https://doi.org/10.3390/buildings9080189

Javanroodi, K., & Nik, V. M. (2020). Interactions between extreme climate and urban morphology: Investigating the evolution of extreme wind speeds from mesoscale to microscale. *Urban Climate, 31*, Article 100544. https://doi.org/10.1016/j.uclim.2019.100544

Javanroodi, K., Nik, V. M., & Scartezzini, J. (2021). Quantifying the impacts of urban morphology on modifying microclimate conditions in extreme weather conditions. *Journal of Physics: Conference Series, 2042*(1), Article 012058. https://doi.org/10.1088/1742-6596/2042/1/012058

Jessel, S., Sawyer, S., & Hernández, D. (2019). Energy, Poverty, and Health in Climate Change: A Comprehensive Review of an Emerging Literature. *Frontiers in Public Health, 7*, 00. https://doi.org/10.3389/fpubh.2019.00357

Kallert, A., Egelkamp, R., & Schmidt, D. (2018). High Resolution Heating Load Profiles for Simulation and Analysis of Small Scale Energy Systems. *Energy Procedia, 149*, 122–131. https://doi.org/10.1016/j.egypro.2018.08.176

Kensby, J. (2015). *Buildings as thermal energy storage – Pilot test and large-scale implementation for district heating systems* [Chalmers University of Technology]. https://research.chalmers.se/en/publication/216470.

Kenward, A., & Raja, U. (2014). BLACKOUT: EXTREME WEATHER, CLIMATE CHANGE AND POWER OUTAGES. *Cliamte Central, 23*, 00.

Khoshnoodmotlagh, S., Daneshi, A., Gharari, S., Verrelst, J., Mirzaei, M., & Omrani, H. (2021). Urban morphology detection and it's linking with land surface temperature: A case study for Tehran Metropolis, Iran. *Sustainable Cities and Society, 74*, 00. https://doi.org/10.1016/j.scs.2021.103228. Scopus.

Kottek, M., Grieser, J., Beck, C., Rudolf, B., & Rubel, F. (2006). World Map of the Köppen-Geiger Climate Classification Updated. *Meteorologische Zeitschrift, 15*, 259–263. https://doi.org/10.1127/0941-2948/2006/0130

Lee, K., Kim, Y., Sung, H. C., Ryu, J., & Jeon, S. W. (2020). Trend analysis of urban heat island intensity according to urban area change in asian mega cities. *Sustainability (Switzerland), 12*(1), 00. https://doi.org/10.3390/su12010112

Li, Y., Zhou, B., Glockmann, M., Kropp, J. P., & Rybski, D. (2021). Context sensitivity of surface urban heat island at the local and regional scales. *Sustainable Cities and Society, 74*, 00. https://doi.org/10.1016/j.scs.2021.103146. Scopus.

Ma, R., Ren, B., Zhao, D., Chen, J., & Lu, Y. (2020). Modeling urban energy dynamics under clustered urban heat island effect with local-weather extended distributed adjacency blocks. *Sustainable Cities and Society, 56*, 00. https://doi.org/10.1016/j.scs.2020.102099. Scopus.

Massana, J., Pous, C., Burgas, L., Melendez, J., & Colomer, J. (2015). Short-term load forecasting in a non-residential building contrasting models and attributes. *Energy and Buildings, 92*, 322–330. https://doi.org/10.1016/j.enbuild.2015.02.007

Masters, J. (2021, August 13). *July 2021 was Earth's warmest month in recorded history, says NOAA » Yale Climate Connections*. Yale Climate Connections. http://yaleclimateconnections.org/2021/08/july-2021-was-earths-warmest-month-in-recorded-history-says-noaa/.

Menberg, K., Heo, Y., & Choudhary, R. (2016). Sensitivity analysis methods for building energy models: Comparing computational costs and extractable information. *Energy and Buildings, 133*, 433–445. https://doi.org/10.1016/j.enbuild.2016.10.005

Mihaela, B. (2014). Implications of Human Settlements Evolution. *Procedia Economics and Finance, 10*, 190–196. https://doi.org/10.1016/S2212-5671(14)00293-7

Moazami, A., Nik, V. M., Carlucci, S., & Geving, S. (2019). Impacts of future weather data typology on building energy performance – Investigating long-term patterns of climate change and extreme weather conditions. *Applied Energy, 238*, 696–720. https://doi.org/10.1016/j.apenergy.2019.01.085. Scopus.

Mourshed, M. (2011). The impact of the projected changes in temperature on heating and cooling requirements in buildings in Dhaka. *Bangladesh. Applied Energy, 88*(11), 3737–3746. https://doi.org/10.1016/j.apenergy.2011.05.024

Naboni, E., Meloni, M., Makey, Chris, & Kämpf, J. (2019). *The Simulation of Mean Radiant Temperature in Outdoor Conditions: A review of Software Tools Capabilities*. 3234–3241. https://doi.org/10.26868/25222708.2019.210301.

Nik, V. M. (2016). Making energy simulation easier for future climate—Synthesizing typical and extreme weather data sets out of regional climate models (RCMs). *Applied Energy, 177*, 204–226. https://doi.org/10.1016/j.apenergy.2016.05.107. Scopus.

Nik, V. M. (2017). Application of typical and extreme weather data sets in the hygrothermal simulation of building components for future climate – A case study for a wooden frame wall. *Energy and Buildings, 154*, 30–45. https://doi.org/10.1016/j.enbuild.2017.08.042. Scopus.

Nik, V. M., & Moazami, A. (2021). Using collective intelligence to enhance demand flexibility and climate resilience in urban areas. *Applied Energy, 281*, 00. https://doi.org/10.1016/j.apenergy.2020.116106. Scopus.

Nik, V. M., Perera, A. T. D., & Chen, D. (2021). Towards climate resilient urban energy systems: A review. *National Science Review, 8*(nwaa134). https://doi.org/10.1093/nsr/nwaa134.

Nik, V. M., & Sasic Kalagasidis, A. (2013). Impact study of the climate change on the energy performance of the building stock in Stockholm considering four climate uncertainties. *Building and Environment, 60*, 291–304. https://doi.org/10.1016/j.buildenv.2012.11.005

NOAA. (2021, August 13). It's Official: July Was Earth's Hottest Month on Record. https://www.noaa.gov/news/its-official-july-2021-was-earths-hottest-month-on-record.

Perera, A. T. D., Javanroodi, K., & Nik, V. M. (2021a). Climate resilient interconnected infrastructure: Co-optimization of energy systems and urban morphology. *Applied Energy, 285*, 00. https://doi.org/10.1016/j.apenergy.2020.116430. Scopus.

Perera, A. T. D., Nik, V. M., Chen, D., Scartezzini, J.-L., & Hong, T. (2020). Quantifying the impacts of climate change and extreme climate events on energy systems. *Nature Energy, 5*(2), 150–159. https://doi.org/10.1038/s41560-020-0558-0. Scopus.

Pezzutto, S., Croce, S., Zambotti, S., Kranzl, L., Novelli, A., & Zambelli, P. (2019). Assessment of the Space Heating and Domestic Hot Water Market in Europe—Open Data and Results. *Energies, 12*(9), 1760. https://doi.org/10.3390/en12091760

Revi, A., Satterthwaite, D. E., Aragón-Durand, F., Corfee-Morlot, J., Kiunsi, R. B. R., Pelling, M., Roberts, D. C., & Solecki, W. (2014). Urban areas. In *Climate Change 2014: Impacts, Adaptation, and Vulnerability. Part A: Global and Sectoral Aspects. Contribution of Working Group II to the Fifth Assessment Report of the Intergovernmental Panel on Climate Change [Field, C.B., V.R. Barros, D.J. Dokken, K.J. Mach, M.D. Mastrandrea, T.E. Bilir, M. Chatterjee, K.L. Ebi, Y.O. Estrada, R.C. Genova, B. Girma, E. S. Kissel, A.N. Levy, S. MacCracken, P.R. Mastrandrea, and L.L. White (eds.)]*. (pp. 535–612). Cambridge University Press, Cambridge, United Kingdom and New York, NY, USA.

Rizwan, A. M., Dennis, L. Y. C., & Liu, C. (2008). A review on the generation, determination and mitigation of Urban Heat Island. *Journal of Environmental Sciences, 20*(1), 120–128. https://doi.org/10.1016/S1001-0742(08)60019-4

Robine, J.-M., Cheung, S. L. K., Le Roy, S., Van Oyen, H., Griffiths, C., Michel, J.-P., & Herrmann, F. R. (2008). Death toll exceeded 70,000 in Europe during the summer of 2003. *Comptes Rendus Biologies, 331*(2), 171–178. https://doi.org/10.1016/j.crvi.2007.12.001

Rogelj, J., den Elzen, M., Höhne, M., Franzen, T., Fekete, H., Winkler, H., Schaeffer, R., Sha, F., Riahi, K., & Meinshausen, M. (2016). Paris Agreement climate proposals need a boost to keep warming well below 2°C. *Nature, 534*, 631–639. https://doi.org/10.1038/nature18307

Ruiz, G. R., & Bandera, C. F. (2017). Validation of Calibrated Energy Models: Common Errors. *Energies, 10*(10), 1587. https://doi.org/10.3390/en10101587

Ryu, Y.-H., & Baik, J.-J. (2012). Quantitative Analysis of Factors Contributing to Urban Heat Island Intensity. *Journal of Applied Meteorology and Climatology, 51*, 842–854. https://doi.org/10.1175/JAMC-D-11-098.1

SCB. (2017). *Over 4.8 million dwellings in Sweden*. Statistiska Centralbyrån. http://www.scb.se/en/finding-statistics/statistics-by-subject-area/housing-construction-and-building/housing-construction-and-conversion/dwelling-stock/pong/statistical-news/dwelling-stock-2017-12-31/.

SCB. (2019). *Official statistics of Sweden – Annual Report 2018*. SCB, Statistiska centralbyrån Statistics Sweden. https://www.scb.se/globalassets/sam-forum/officiell-statistik/sos-rapporter/official-statistics-annual-report-2018.pdf.

Schiefelbein, J., Rudnick, J., Scholl, A., Remmen, P., Fuchs, M., & Müller, D. (2019). Automated urban energy system modeling and thermal building simulation based on OpenStreetMap data sets. *Building and Environment, 149*, 630–639. https://doi.org/10.1016/j.buildenv.2018.12.025

Schwartz, J. (2005). Who is sensitive to extremes of temperature?: A case-only analysis. *Epidemiology (Cambridge, Mass.), 16*(1), 67–72. https://doi.org/10.1097/01.ede.0000147114.25957.71

Sethi, M., Sharma, R., Mohapatra, S., & Mittal, S. (2021). How to tackle complexity in urban climate resilience? Negotiating climate science, adaptation and multi-level governance in India. *PLoS ONE, 16*(7 July), 00. https://doi.org/10.1371/journal.pone.0253904. Scopus.

Seto, K. C., Dhakal, S., Bigio, A., Blanco, H., Delgado, G. C., Dewar, D., Huang, L., Inaba, A., Kansal, A., Lwasa, S., McMahon, J. E., Müller, D. B., Murakami, J., Nagendra, H., & Ramaswami, A. (2014). Human Settlements, Infrastructure and Spatial Planning. In *Climate Change 2014: Mitigation of Climate Change Contribution of Working Group III to the Fifth Assessment Report of the Intergovernmental Panel on Climate Change [Edenhofer, O.,R. Pichs-Madruga, Y.Sokona, E.Farahani, S.Kadner, K.Seyboth, A.Adler, I.Baum, S.Brunner, P.Eickemeier, B.Kriemann, J.Savolainen, S.Schlömer, C.von Stechow, T.Zwickel and J.C.Minx (eds.)]*. Cambridge University Press, Cambridge, United Kingdom and New York, NY, USA.

Sørensen, L. (2013). Heat Transmission Coefficient Measurements in Buildings Utilizing a Heat Loss Measuring Device. *Sustainability, 5*(8), 3601–3614. https://doi.org/10.3390/su5083601

Sousa, J. (2012). Energy simulation software for buildings: Review and comparison. *International Workshop on Information Technology for Energy Applicatons-IT4Energy, Lisabon*.

Taha, H. (1997). Urban climates and heat islands: Albedo, evapotranspiration, and anthropogenic heat. *Energy and Buildings, 25*(2), 99–103. https://doi.org/10.1016/S0378-7788(96)00999-1

Thomson, H., Simcock, N., Bouzarovski, S., & Petrova, S. (2019). Energy poverty and indoor cooling: An overlooked issue in Europe. *Energy and Buildings, 196*, 21–29. https://doi.org/10.1016/j.enbuild.2019.05.014

Tian, W., Heo, Y., de Wilde, P., Li, Z., Yan, D., Park, C. S., Feng, X., & Augenbroe, G. (2018). A review of uncertainty analysis in building energy assessment. *Renewable and Sustainable Energy Reviews, 93*, 285–301. https://doi.org/10.1016/j.rser.2018.05.029. Scopus.

Tsoka, S., Tolika, K., Theodosiou, T., & Tsikaloudaki, K. (2017). Evaluation of stochastically generated weather datasets for building energy simulation. *Energy Procedia, 122*, 853–858. https://doi.org/10.1016/j.egypro.2017.07.449

Ueno, T., & Meier, A. (2020). A method to generate heating and cooling schedules based on data from connected thermostats. *Energy and Buildings, 228*. Scopus. https://doi.org/10.1016/j.enbuild.2020.110423.

UN. (2015). *Transforming our World: The 2030 Agenda for Sustainable Development .:. Sustainable Development Knowledge Platform*. https://sustainabledevelopment.un.org/post2015/transformingourworld/publication.

Walch, A., Castello, R., Mohajeri, N., & Scartezzini, J.-L. (2020). Big data mining for the estimation of hourly rooftop photovoltaic potential and its uncertainty. *Applied Energy, 262*, Article 114404. https://doi.org/10.1016/j.apenergy.2019.114404

Wang, C., Wei, S., Du, S., Zhuang, D., Li, Y., Shi, X., Jin, X., & Zhou, X. (2021). A systematic method to develop three dimensional geometry models of buildings for urban building energy modeling. *Sustainable Cities and Society, 71*, Article 102998. https://doi.org/10.1016/j.scs.2021.102998

Wei, Y., Zhang, X., Shi, Y., Xia, L., Pan, S., Wu, J., Han, M., & Zhao, X. (2018). A review of data-driven approaches for prediction and classification of building energy consumption. *Renewable and Sustainable Energy Reviews, 82*, 1027–1047. https://doi.org/10.1016/j.rser.2017.09.108

Yang, Y., Javanroodi, K., & Nik, V. M. (2021). Climate change and energy performance of European residential building stocks – A comprehensive impact assessment using climate big data from the coordinated regional climate downscaling experiment. *Applied Energy, 298*, Article 117246. https://doi.org/10.1016/j.apenergy.2021.117246

Zhao, H., & Magoulès, F. (2012). A review on the prediction of building energy consumption. *Renewable and Sustainable Energy Reviews, 16*(6), 3586–3592. https://doi.org/10.1016/j.rser.2012.02.049

Zhou, Y., Zhang, G., Jiang, L., Chen, X., Xie, T., Wei, Y., Xu, L., Pan, Z., An, P., & Lun, F. (2021). Mapping local climate zones and their associated heat risk issues in Beijing: Based on open data. *Sustainable Cities and Society, 74*, 00. https://doi.org/10.1016/j.scs.2021.103174. Scopus.

Zoras, S., Veranoudis, S., & Dimoudi, A. (2017). Micro- climate adaptation of whole building energy simulation in large complexes. *Energy and Buildings, 150*, 81–89. https://doi.org/10.1016/j.enbuild.2017.05.060. Scopus.